Two-step deswelling in the Volume Phase Transition of thermoresponsive microgels

Giovanni Del Monte, Domenico Truzzolillo, Fabrizio Camerin, Andrea Ninarello, Edouard Chauveau, Letizia Tavagnacco, Nicoletta Gnan, Lorenzo Rovigatti, Simona Sennato, Emanuela Zaccarelli

Two-step deswelling in the Volume Phase Transition of thermoresponsive microgels

Giovanni Del Monte,[1,2,3] Domenico Truzzolillo,[4,a)] Fabrizio Camerin,[2,1] Andrea Ninarello,[2,1] Edouard Chauveau,[4] Letizia Tavagnacco,[2,1] Nicoletta Gnan,[2,1] Lorenzo Rovigatti,[1,2] Simona Sennato,[2,1] and Emanuela Zaccarelli[2,1,b)]

[1)]*Department of Physics, Sapienza University of Rome, p.le A. Moro 2 00185 Roma, Italy*
[2)]*CNR-ISC, Sapienza University of Rome, p.le A. Moro 2, 00185 Roma, Italy*
[3)]*CLNS, Istituto Italiano di Tecnologia, v.le Regina Elena 291, 00161 Roma, Italy*
[4)]*Laboratoire Charles Coulomb (L2C), UMR 5221 CNRS-Universitè de Montpellier, 4 F-34095 Montpellier, France*

(Dated: 22 April 2021)

Thermoresponsive microgels are one of the most investigated class of soft colloids, thanks to their ability to undergo a Volume Phase Transition (VPT) close to ambient temperature. However, this fundamental phenomenon still lacks a detailed microscopic understanding, particularly regarding the presence and the role of charges in the deswelling process. Here we fill this gap by combining experiments and simulations to show that the microgel collapse does not happen in a homogeneous fashion, but through a two-step mechanism, entirely attributable to electrostatic effects. The signature of this phenomenon is the emergence of a minimum in the ratio between gyration and hydrodynamic radii at the VPT. Thanks to simulations of several microgels with different cross-linker concentrations, charge contents and charge distributions, we build a unifying master-curve able to predict the two-step deswelling. Our results have direct relevance on fundamental soft condensed matter science and on microgel applications ranging from materials to biomedical technologies.

PACS numbers: 82.20.Wt 61.25.Hq

INTRODUCTION

Responsive particles have recently captured the interest of scientists working under many diverse fields[1–4]. Indeed, their ability to adapt to the environmental conditions has enormous advantages for potential applications from biochemistry to nanomedicine[5–8], but also as smart sensors for various analytes[9–11]. The versatility of these soft objects lies in the manifold routes in which the chemical components can be synthesized and in the transfer of the single-particle properties to the mesoscopic and macroscopic level.

In particular, most of these responsive particles are macromolecular colloids, whose inner structure relies on a polymeric system which controls the behavior at the colloidal scale. The prototypical example, that is most actively studied in the literature nowadays, is that of microgel particles, i.e. colloidal-scale realizations of a crosslinked polymer network[12,13]. In their most elementary version, these microgels are composed by a single monomeric component. Among all possible polymers, Poly(N-isopropylacrylamide) (pNIPAM) is thermoresponsive and undergoes a solubility transition from good to bad solvent conditions at a temperature $T_c \sim 32$°C. The counterpart of this phenomenon for pNIPAM microgels is called Volume Phase Transition (VPT), by which particles are able to reversibly swell and de-swell across T_c.

Microgels can be routinely synthesized in a wide range of sizes roughly going from 50 nm to 100 µm in diameter, reason for which they are applicable to a variety of purposes and can be investigated with different experimental techniques, from neutron[14] and x-ray scattering[15] up to optical methods and microfluidics[16]. In addition, their complex internal structure and collective behaviour, involving particle deformation and interpenetration, can nowadays be resolved with single-particle detail thanks to recent advancements in super-resolution microscopy[17–20]. The possibility to be studied with these fascinating tools make them also one of the favorite model systems for fundamental science both in bulk suspensions[13,21] and adsorbed at interfaces[22–25].

For all the above reasons, it is legitimate to say that the volume phase transition occurring in pNIPAM microgels is one of the most studied phenomena in soft condensed matter. Despite the huge amount of experimental and theoretical work on this topic, that is witnessed by the large number of recent reviews[26–33], there are still fundamental aspects of the VPT that remain poorly understood. In particular, pNIPAM microgels are often treated as neutral systems, since electrostatic interactions are usually thought not to play an important role in their behaviour, apart from the stabilization against aggregation given to the suspension. However, the typical batch synthesis procedure of pNIPAM microgels usually includes charged compounds, in particular those from the initiators of the polymerisation process. While their presence may be effectively neglected or screened out by the addition of salt[15], there are recent works that pointed out a relevant effect of peripheral charges in concentrated suspensions[34]. At present, the influence of these charges on the VPT has not been clarified yet.

One of the reasons for which these aspects have not been investigated so far may be the lack of detailed numerical simulations able to treat a single microgel in a realistic way. To address these gaps, we recently developed a computa-

[a)]domenico.truzzolillo@umontpellier.fr
[b)]emanuela.zaccarelli@cnr.it

tional method[35] to assemble disordered networks with desired crosslinker concentration and a core-corona structure that closely reproduces experimental behaviour[15,36]. After imposing the correct internal structure, we extended our method to properly include the presence of charged monomers with explicit counterions[37], again validating our results in the presence of explicit solvent and comparing with available experiments[38]. For these reasons, we are now in the condition to carefully assess the effect of initiator charges on the deswelling mechanism of pNIPAM microgels across the VPT.

By combining simulations with static and dynamic light scattering experiments, here we show that the presence of these charges strongly affects, from a qualitative point of view, the deswelling transition, inducing an inhomogeneous two-step collapse of the microgels with increasing temperature. This is due to the different solvophobicity of pNIPAM and charged groups, respectively, which manifests in the emergence of a minimum in the ratio between the gyration R_g and hydrodynamic R_H radii at the VPT. First of all, we show that such a minimum is absent for neutral microgels. Second, we analyse in detail the role of the charge distribution throughout the microgel network. In this way, we provide evidence that the initiator groups are preferentially located on the surface of the microgels, as previously hypothesized[34], but never directly proven so far. In order to be able to predict the onset of the two-step deswelling, we further study different combinations of degree of crosslinking, microgel size and charge distribution, establishing clear trends in the occurrence of the minimum in R_g/R_H with increasing charge content and decreasing crosslinker concentration. Notably, we finally obtain a master-curve for the observed minimum for all simulated microgels when we plot it as a function of the average charge content per chain on the microgel surface, which turns out to be the simplest indicator of the presence of the two-step collapse.

Our work sheds light on the fundamental electrostatic interactions influencing microgel deswelling, which are crucial to correctly describe their assembly and collective behaviour at high temperatures. In addition, it opens up the possibility to *a priori* design microgels with desired characteristics and tunable onset of two-step deswelling, which could be exploited to enhance or adjust the potential applications of microgels as smart micro-objects.

RESULTS

Experimental results: swelling curves and R_g/R_H

The ratio between gyration and hydrodynamic radii is a relevant quantity in polymer science, widely used as a shape index[39–41]. These two lengths differently characterize the average polymer distribution inside the macromolecular volume. While R_g is the radius obtained from the standard deviation of the mass distribution around the centre of mass, R_H is an effective size extracted from the self-diffusion coefficient $\bar{D}$ of the particle. For hard spheres (HS) moving in an ideal continuous solvent, considering a uniform distribution of the mass within the particle, a value of $R_g/R_H \approx 0.77$ is found[42]. For pNIPAM microgels obtained through radical polymerisation, this quantity at low T is usually smaller than the HS value[43], since particles consist of a denser core with a density profile gradually fading into the corona. The latter is characterized by the presence of long external chains, the so-called dangling ends, that eventually manifest in an increase of the measured R_H, because of their contribution to the drag, but would not affect the value of R_g[44]. At high temperatures, instead, where microgels are completely collapsed, the ratio should tend to the homogeneous HS limit. Since these two lengths carry complementary information, it is instructive to compare their behaviour for microgels across the VPT, in particular to capture the occurrence of internal inhomogeneities of the macromolecular structure upon collapse.

We start by showing experimental results for the size variation of microgels in Fig. 1, where both R_g (a) and R_H (b) are reported as a function of temperature T for the different microgel suspensions investigated in this work. We consider pNIPAM microgels synthesized with a fixed amount of potassium persulfide (KPS), which brings into the network a negative charge for each radical unit used in the polymerisation reaction. We use a reference sample (i) with a molar fraction of KPS equal to $I_{\mathrm{KPS}} = 1.6\%$ and a crosslinker concentration $c = 5.25\%$, in surfactant free conditions, while varying crosslinker content, initiator content and type respectively for three other samples, to systematically assess the effect of each aspect. Namely, we also investigate: (ii) $I_{\mathrm{KPS}} = 1.6\%$ and $c = 1.37\%$ (with added surfactant, see Methods), primarily to assess the role of crosslinker; (iii) I_{KPS}=8.0% and $c = 5.25\%$ to evaluate the role of the amount of initiator; (iv) microgels where ammonium persulfide (APS) instead of KPS, is used as initiatior, giving the same charge to the polymer network and differing only on the counterion species (NH_3^+ versus K^+). For the latter case, the amount of initiator and crosslinker are the same as in the reference sample ($I_{\mathrm{APS}} = 1.6\%$, $c = 5.25\%$).

We observe in Fig. 1(a) that both $c = 5.25\%$ samples with initiator amount of 1.6% have a comparable gyration radius, of roughly 150 nm. Instead, the sample with enhanced KPS amount has a much larger gyration radius ($\sim$ 250 nm). Concerning the hydrodynamic radius, we find that all three samples with c=5.25% are found to have a comparable size, close to 300 nm, and a similar swelling ratio roughly equal to 2. We notice as well that microgels with c=1.37% are sensibly smaller, due to the addition of surfactant, and display a larger swelling ratio, as expected for loosely crosslinked microgels. From the swelling curves, we estimate the VPT temperature T_c using a phenomenological function, as described in the Supplementary Material (SM). First, we find that the VPT temperature associated to R_g depends on the amount of initiator, since $T_c \sim 31$°C for $I_{\mathrm{KPS,APS}} = 1.6\%$, while it is ≈ 2°C higher for $I_{\mathrm{KPS}} = 8\%$. This result can be rationalized by considering the electric charge brought by initiator molecules. Indeed, in agreement with previous studies on charged microgels[38,45], a shift of T_c to higher values is found when the amount of charges increases. Second, we observe that, for all studied samples, the VPT transition is encountered at a lower tem-

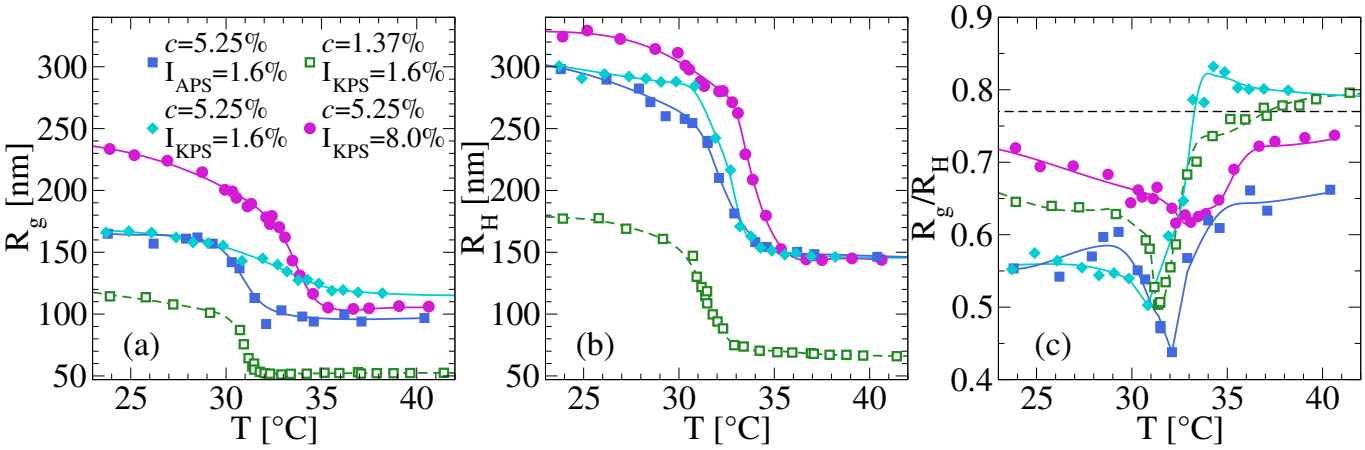

FIG. 1. **Swelling curves and R_g/R_H from experiments.** (a) Gyration radius R_g, (b) hydrodynamic radius R_H and (c) ratio between gyration and hydrodynamic radius R_g/R_H as a function of temperature. Symbols are experimental data, while lines are guides to the eye. The dashed line in panel (c) indicates the HS value for R_g/R_H. For the sake of clarity we do not report error bars. The values of R_g, and by consequence R_g/R_H, are affected by a relative error not exceeding the 30% of the best-fit values for the swollen microgels synthesized in absence of surfactant, while the uncertainty is less than 10% for collapsed microgels and for the smallest microgels in the entire temperature range investigated here (see Methods).

perature, by ≈ 1.0°C, for R_g with respect to R_H. This could be tentatively interpreted in terms of the presence of charged molecules preferentially within the surface of the network, as previously hypothesized[46], an aspect that will be further analyzed later.

Fig. 1(c) shows R_g/R_H as a function of T for all samples. At low temperatures, all studied microgels display a lower ratio with respect to the HS limit, indicating a less homogeneous mass distribution. We observe a higher value for R_g/R_H both for loosely crosslinked microgels (c=1.37%) and for those that carry a high amount of charges ($I_{\mathrm{KPS}} = 8\%$). The fact that in the former case the particles have a more compact shape, as suggested by the value of R_g/R_H at low T, may be caused by the presence of surfactants. Instead, for the latter case the larger number of chain ends (constituted by the initiator molecules) may result in shorter chains, which, combined with the small crosslinking effect of KPS[47], may lead to higher monomers density in the corona, thus giving rise to more homogeneous particles. However, for large T, microgels become compact and all curves tend to converge toward the homogeneous HS value. Although experimental uncertainties prevent us from drawing conclusions on the specific values and trends observed for the different samples, we clearly identify that all samples display a minimum in R_g/R_H close to the VPT temperature estimated from the hydrodynamic radius (see Table S1). In particular, the three microgels with the same initiator amount display a minimum close to $T_c \sim 32$°C, which is instead found at a slightly larger temperature for microgels with $I_{\mathrm{KPS}} = 8\%$. Interestingly, in this case, the minimum is rather shallow, as opposed to those of the other samples where it is more pronounced.

The presence of a minimum in R_g/R_H has been previously observed in a few experimental studies[48,49], including one from some of the present authors[50] for large and loosely crosslinked microgels. Most of these previous studies reported only a few data points around the VPT, so that the presence of the minimum was hinted, but not totally evident. In the present work, the fine resolution in temperature allows us to unambiguously observe the minimum for all samples. Such a minimum in R_g/R_H can be interpreted in terms of a non-uniform collapse of the microgels, that could be intuitively attributed to the underlying inhomogeneous core-corona structure of the microgels. However, an alternative explanation could be found in the role played by the initiator charged groups on the deswelling behaviour[34,50]. In particular, arguments in favour of a specific distribution of these charges have been put forward[46,51,52], suggesting that during polymerisation, the charged groups try to minimize their mutual electrostatic repulsion by remaining far from each other, thus being located mostly at the periphery rather than in the core of the microgels. However, no direct evidence for the location and the arrangement of these groups has been provided so far. This hypothesis certainly needs further investigation, as discussed in the following sections.

Numerical results: unveiling the role of charges

To provide a microscopic understanding of this issue, we rely on numerical simulations. We focus on microgels that closely match the experimental ones, by imposing very similar crosslinking contents, namely c=1.25% and 5%. We compare the case of perfectly neutral microgels with charged ones, having the same charged monomers fraction ($f = 3.2\%$) as the initiator groups in experimental systems. For this specific value of f, we also vary the charge distribution by considering a random arrangement of the charges either throughout the network, hereafter named *random charge distribution*, or only onto surface chains (see Methods), that we refer to as *surface*

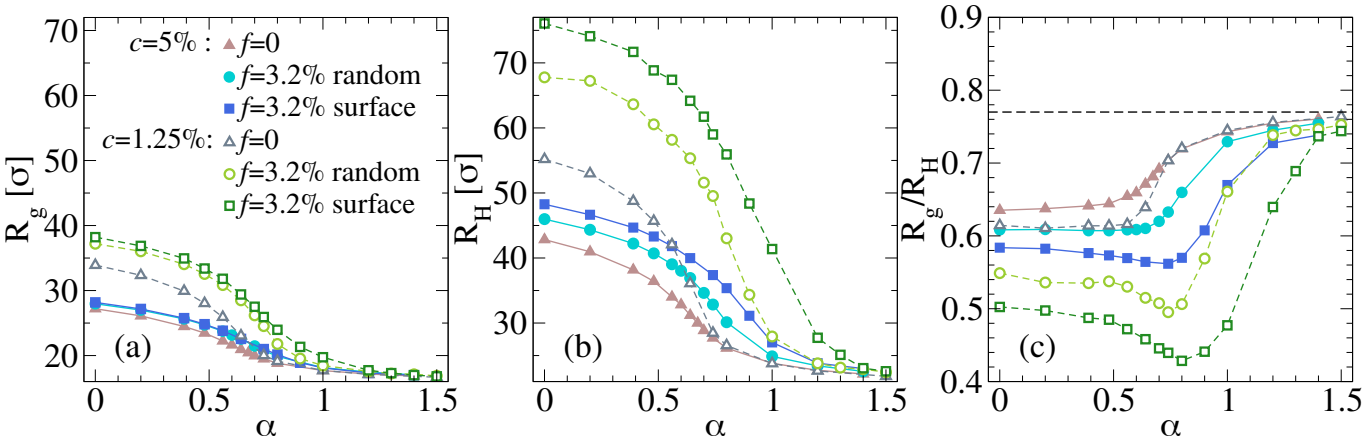

FIG. 2. **Swelling curves and R_g/R_H from simulations.** (a) Gyration radius R_g, (b) hydrodynamic radius R_H and (c) ratio between gyration and hydrodynamic radius R_g/R_H as a function of the solvophobic parameter α for microgels with $N \sim 42K$ monomers at comparable crosslinker concentrations used in experiments, $c = 1.25\%$ (open symbols) and $c = 5.0\%$ (closed symbols). Data refer to neutral microgels ($f = 0$, triangles) and to charged microgels with $f = 0.032$, corresponding to the initiator amount in experiments, but with two different charge distributions: random (circles) and surface (squares), as described in the text. The horizontal dashed line indicates the corresponding HS value.

charge distribution. In this way, we are able to assess how the deswelling behaviour is affected by the charge arrangement upon increasing temperature.

Our modelling is based on a coarse-grained representation of a disordered microgel network with a realistic core-corona distribution, that is able to faithfully reproduce experimental form factors across the VPT[15]. In the presence of charges, our treatment explicitly includes the presence of counterions, as these turn out to be crucial to provide a proper description of the local inhomogeneities arising in the network[37]. In addition, charged monomers do not change their affinity to the solvent as we vary the temperature in order to properly capture the experimental situation[38]. A detailed description of the model is provided in Methods.

Numerical results for the radius of gyration R_g of the microgels are reported in Fig. 2(a) as a function of the solvophobic parameter α, which plays the role of an effective temperature in simulations. As expected, the gyration radius is found to be mostly influenced by the crosslinker concentration, with R_g being much larger for $c = 1.25\%$ than for $c = 5\%$. On the other hand, the presence of charges has a small effect on the gyration radius, which increases only slightly with f. Notably, the effect of charge arrangement within the network is almost absent, being R_g very similar for random and surface distributions.

The estimates of the hydrodynamic radius for the *in silico* microgels, as defined in Methods, are reported in Fig. 2(b) as a function of the solvophobic parameter α, displaying a behaviour that looks rather similar to that of R_g. An important difference, however, arises when comparing the two different charge distributions. Indeed, we find a significant increase of R_H in the presence of a surface charge distribution compared to the case with random charges due to the accumulation of charges in the corona of the microgel which keeps the latter much more expanded.

Having calculated both gyration and hydrodynamic radii, it is now possible to examine the ratio R_g/R_H also in simulations. This is shown in Fig. 2(c) as a function of α. First of all, we notice that our numerical definition of R_H allows us to obtain estimates for the ratio R_g/R_H that are, within statistical uncertainties, in reasonable agreement with experimental ones and that correctly tend to the HS value at large α in all cases. While we observe the emergence of a minimum in R_g/R_H under specific conditions of charge content f and charge distribution, it is important to highlight that such a minimum is totally absent for perfectly neutral microgels, independently of the value of c. This result allows us to unambiguously exclude that the appearance of the minimum stems from the underlying core-corona topology of the microgels. Rather, it turns out to be related to the presence of the initiator charges, which therefore plays an explicit role in the VPT of pNIPAM microgels. Such a role, not often recognized in the literature up to now, appears to be important to properly capture the internal modifications of the microgels upon collapse. This is also confirmed by electrophoretic mobility measurements across the VPT for a subset of the samples investigated in this work, as reported in Fig. S1 and also previously discussed in Refs.[50,53].

By examining in more detail the specific features of the microgel for which a minimum in R_g/R_H is present, we find that, for both studied values of c, microgels with charges arranged on the surface display a very pronounced minimum that occurs roughly at the VPT in agreement with experimental findings. Instead, for randomly located charges, the presence of a minimum is evident only for c=1.25%, while it is absent for $c = 5.0\%$. Since a minimum is observed for all samples in experiments, this suggests that initiator charges are not randomly spread throughout the network, but rather they are preferentially located close to the microgel surface.

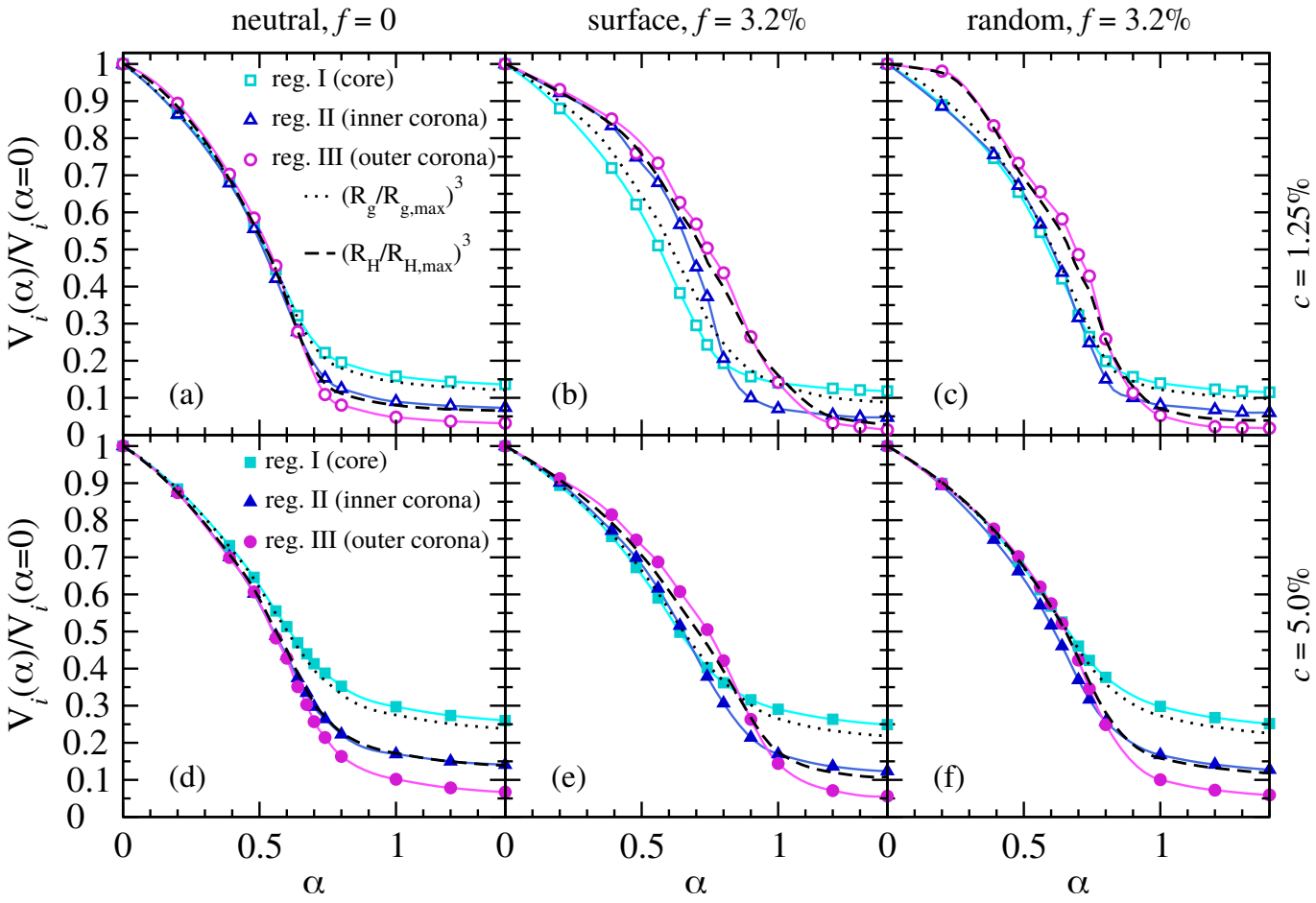

FIG. 3. **Local swelling curves.** Normalized volume for the three different regions, defined as $V_i(\alpha)/V_i(0)$ where V_i refers to the volume of the ith region, labeled as i =I, II, III for core, inner and outer corona regions, respectively. Panels in the top row refer to microgels with $c = 1.25\%$ and different charge realizations: (a) neutral ($f = 0$), (b) surface charge distribution ($f = 3.2\%$) and (c) random charge distribution ($f = 3.2\%$). Panels in the bottom row refer to microgels with $c = 5.0\%$ and different charge realizations: (d) neutral ($f = 0$), (e) surface charge distribution ($f = 3.2\%$) and (f) random charge distribution ($f = 3.2\%$). Black lines are obtained from evaluating the volume ratio of spherical regions corresponding to the gyration radius (dotted line) and to the hydrodynamic radius (dashed lines).

Microscopic origin of the two-step collapse

In order to unveil the microscopic mechanism that gives rise to the presence of a minimum in R_g/R_H, we analyse the microgels by selecting different regions within their volume and calculating their relative swelling in a so-called "local swelling" approach. In order to define the internal regions, we fix the number of particles within each region and assign them on the basis of their distance from the centre of mass. In this way, upon varying α, we monitor the true volume variation of a given portion of the microgel. The three regions are defined as follows: (region I) the *core* region roughly having the same volume as a sphere of radius equal to the gyration radius; (region II) the *inner corona* region, corresponding to an intermediate shell, whose volume —together with that of the core— roughly coincides with that delimited by the hydrodynamic radius, and (region III) the *outer corona* shell. More details on the choices of the three regions are given in Methods and in the SM (see Fig. S2).

We start by discussing the behaviour of the neutral microgel. For both values of the examined crosslinked concentrations, reported in Fig. 3(a) and (d), we observe that the deswelling transition, monitored by the volume change of each region, occurs roughly at the same value of the solvophobic parameter for all regions. These results indicate that a purely neutral microgel deswells in a homogeneous fashion, independently on the internal structure and thus on its intrinsic core-corona topology. This is due to the fact that all monomers experience the same affinity to the solvent, which induces a simultaneous collapse of the whole particle. No difference is observed between the two values of c, except for a more pronounced swelling ratio for the less crosslinked microgels, as expected.

We now turn to the surface-charged microgel with $f = 3.2\%$, whose local swelling behaviour is reported in Fig. 3(b) and (e). In this case, it is evident that the collapse of the three regions does not occur simultaneously, with the core (region I) showing a deswelling transition which takes place at a sen-

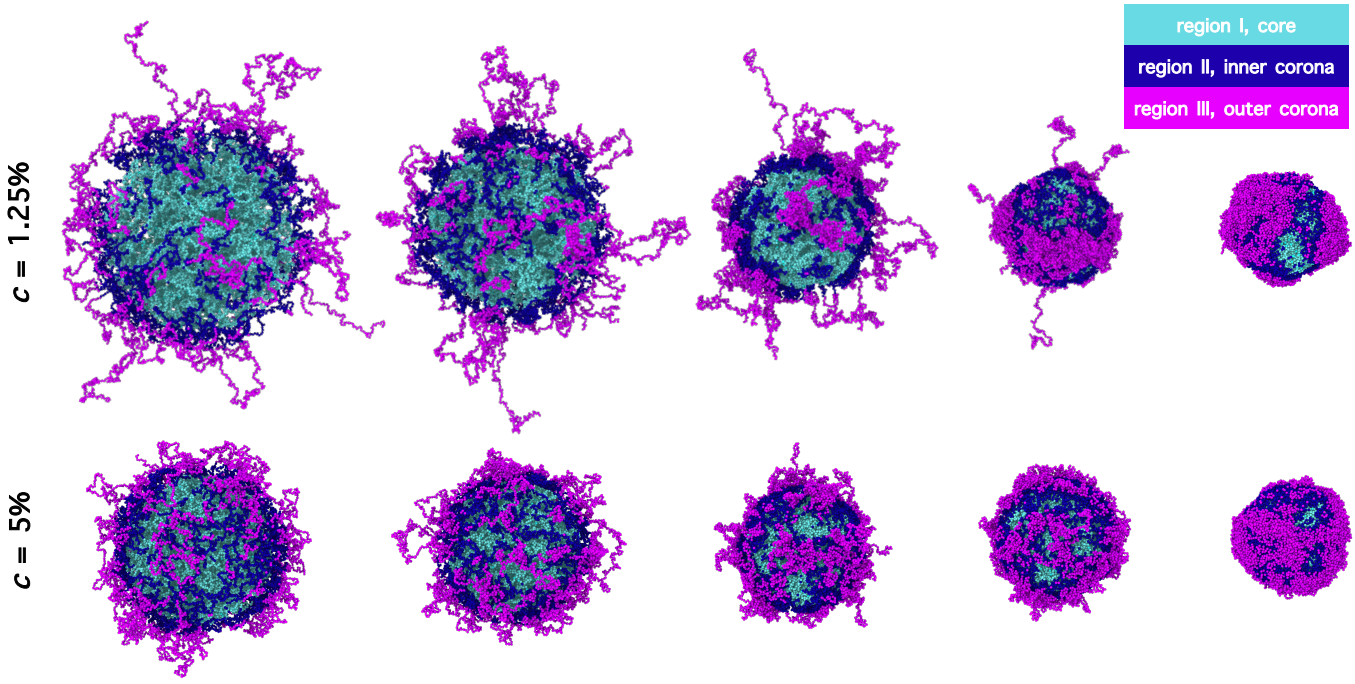

FIG. 4. **Snapshots of randomly charged microgels across the VPT illustrating the local swelling** Simulation snapshots for randomly-charged microgel ($f = 3.2\%$) with two values of crosslinker concentration c for different values of the swelling parameter α from the swollen to the collapsed state. From left to right, for $c = 1.25\%$, $\alpha = 0, 0.48, 0.74, 0.90, 1.20$, while for $c = 5\%$, $\alpha = 0, 0.48, 0.74, 0.80, 1.20$. Monomers are colored according to the region they belong to: cyan indicate the core region, blue the inner corona region and purple the outer corona region. All snapshots refer to equilibrium states.

sibly lower value of α with respect to the outer corona (region III). In addition, a clear difference is now present for the two values of c regarding the inner corona region (region II): while its collapse is approximately the same as that of the core for $c = 5\%$ (panel e), a clear delay in α is present for the less crosslinked microgel (panel b). In the latter case, a clear sequence of inflection points is found when going from the inner to the outer region. Similarly to the neutral case, we still observe that the behaviour of the sphere of radius R_g roughly follows that of the core, while that of radius R_H is very close to that of the corona region. These results clearly show that the development of a minimum in the ratio between R_g and R_H, as reported in Fig. 2, can be easily interpreted in terms of the different collapse behaviour that involves, respectively, the core and the corona region, the latter intended as a whole.

We thus refer to this phenomenology for simplicity as a 'two-step' collapse, although the number of steps may depend on the level of heterogeneity of the underlying microgel. Its microscopic origin can thus be traced back to the different affinity of the charged monomers with respect to the solvent and to their different electrostatic screening conditions. Indeed, since charges remain solvophilic at all values of α and are accumulated in the corona, this provides the microgel with a heterogeneous collapse mechanism which differentiates the core (where charges are absent) from the corona (where most of the charges are located).

While surface-charged microgels unambiguously show a two-step collapse for both studied c values, the situation is different for randomly-charged microgels with $f = 3.2\%$, reported in Fig. 3(c) and (f). Indeed, these microgels display a different behaviour according to the value of c: while for $c = 1.25\%$ the outer corona is found to undergo a deswelling transition at a larger value of α with respect to the core, this is not the case for $c = 5\%$. This is reflected in the occurrence of a minimum in R_g/R_H only for the randomly charged case with $c = 1.25\%$, while this is absent for $c = 5\%$, as previously shown in Fig. 2(c). To further confirm that the presence of the minimum is associated to a non-homogeneous internal deswelling of the microgels, we report the snapshots of randomly-charged microgels for the two studied c-values in Fig. 4. Starting with the $c = 1.25\%$ microgel, we clearly see that long dangling chains remain in rather extended configurations even when the internal portions of the networks have already collapsed. This is also evident at α values slightly above the VPT, where both core and inner corona are found in a compact spherical shape, while the outer chains are still protruding out of the sphere, giving the microgel an anisotropic global structure. It is instructive to focus on the outer corona monomers at intermediate values of α, where the external chains are formed by a mixture of collapsed and extended regions, due to the different solvophobic interactions of charged and neutral monomers, respectively. Although the charge distribution is random, the large amount of long chains in a low-crosslinked microgel (see Fig. S3) makes it favourable to have several charged groups in these regions. This is responsible for the onset a minimum in R_g/R_H, precisely by the same

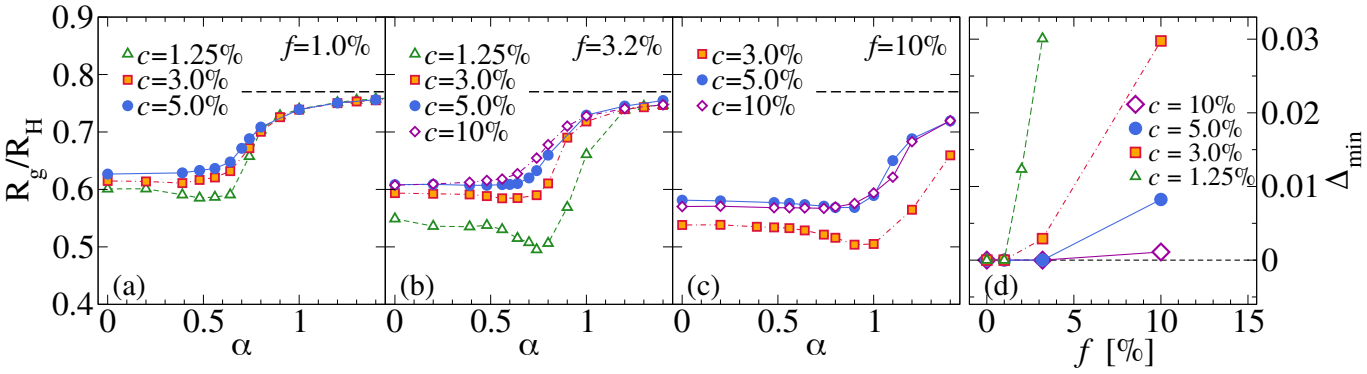

FIG. 5. **Ratio R_g/R_H for randomly-charged microgels** as a function of the solvophobic parameter α for (a) $f = 1.0\%$, (b) $f = 3.2\%$ and (c) $f = 10\%$ and different values of c. Dashed lines indicate the HS value; (d) Depth of the minimum in R_g/R_H, $\Delta_{\min}$, as a function of f for different crosslinker concentrations. The swelling curves referring to R_g and R_H for the microgels shown in panels (a-c) are reported in Fig. S5.

mechanism occurring in surface-charged microgels. However, such behaviour is not observed for $c = 5\%$, where the larger amount of crosslinkers strongly limits the chain length in the corona region, thus inhibiting the mutual influence of charges on the dangling chains. This is clearly visible in the snapshots of Fig. 4, illustrating a rather homogenous deswelling for the $c = 5\%$ randomly charged microgel at all values of α. Furthermore, we notice that around the VPT the external monomers approximately fill the whole surface, completely covering the inner part of the microgel. This is not observed for $c = 1.25\%$ where a large portion of core region is still exposed, signaling a rather anisotropic collapse. For comparison, corresponding snapshots for surface-charged microgels are reported in Fig. S4.

On the basis of the above evidence, we are now able to associate the presence of the minimum in R_g/R_H to the two-step collapse of the microgel, differentiating core and corona behaviour. While the underlying topology is not responsible for the two-step mechanism, it facilitates the onset of the minimum even for randomly-charged microgels at low-crosslinked concentrations, due to the more heterogeneous nature of the network under these conditions.

Effect of crosslinker concentration and charge amount on the minimum in R_g/R_H for randomly charged microgels

In the previous subsection we provided evidence that the presence of charged groups is a necessary condition for the occurrence of a minimum in R_g/R_H, but also that this is found to depend on the specific charge distribution and on the crosslinker concentration. While for microgels decorated with surface charges for $f = 3.2\%$, we observed the minimum for both studied values of c, which can be intuitively understood in terms of the delayed collapse of charged surface chains, the situation turned out to be more complex for randomly-charged microgels. Indeed, in this case, the minimum was found to be either present or absent upon variation of c, as shown in Fig. 2 and explained in Fig. 3. To shed light on this aspect, we now focus on microgels with random charge distributions and investigate the effect of varying f as well as c. The behaviour of R_g/R_H as a function of effective temperature α is reported in Figs. 5(a-c) for a large variety of microgels, with c varying between 1.25% and 10% and f exploring a range from 1% to 10%.

We observe that, upon decreasing c and leaving f unchanged, the minimum becomes more and more evident, in agreement with unpublished experimental results[49]. In addition, Fig. 5 shows that the minimum is more pronounced with increasing f at the same value of c, also shifting to larger and larger values of α. In all cases, the decrease of R_g/R_H at the minimum is also accompanied by its decrease at low α, indicating that the growth of R_H is not compensated by that of R_g under these conditions. At large α most curves tend to recover the HS value, except for the most charged microgels, that are expected to completely collapse at much larger effective temperatures, beyond those explored in the present simulations. This is in agreement with previous studies[38,45] that showed a systematic shift of the VPT temperature with increasing charge content. Indeed, it is important to notice that the present results could be relevant not only for pNIPAM homopolymer microgels, but also for ionic ones, e.g. in the presence of a co-polymer such as polyacrilic acid, where charges should be randomly-located throughout the network, for which a two-step behavior of the R_H swelling curves[54] was reported at high charge content.

From all data in Fig. 5(a), we can build a plot representing the depth of the minimum $\Delta_{\min}$ (defined in Methods) as a function of charge content, reported in Fig. 5(b), for different values of c, identifying regions in the (c, f) parameter space where no minimum is observed (homogeneous deswelling), as opposed to others where this is present (two-step deswelling). Clearly, no minimum is found for low c and low f. However, for very large c, the minimum is also inhibited even for very large charge content, such as 10%. Indeed, the highest charge content usually found in experiments is $\approx 10 \div 20\%$[54,55], being it hard to reach such values for pure pNIPAM microgels, because of the termination effect of the initiator on chains. The latter, probably causing the shortening of the external

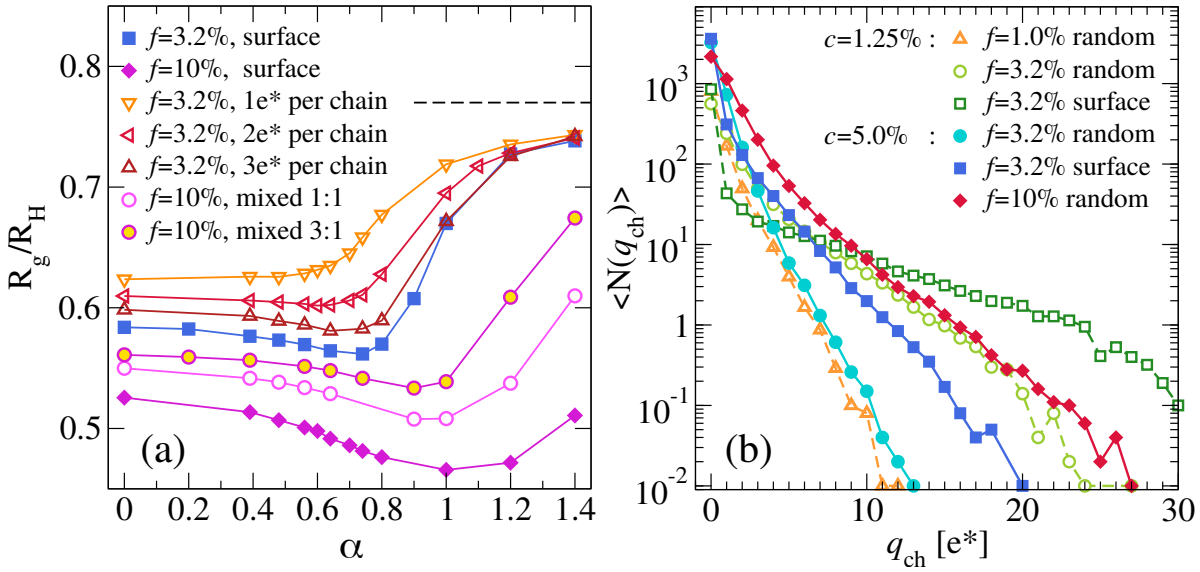

FIG. 6. **Ratio R_g/R_H for c=5% surface-charged microgels and distribution of charges per chain.** (a) R_g/R_H as a function of α for varying charge content and charge distribution. Standard surface-charged microgels are shown with filled symbols. In addition, we show three alternative charge distributions (open triangles) for $f = 3.2\%$ in which the charges are constrained to be found as one, two or three charges on each external chain, indicated as $-1e^*, -2e^*, -3e^*$ per chain, respectively. For $f = 10\%$ we also report results for "mixed" charge distribution (open circles) where part of the charges (50% in the case 1:1 and 75% in the case 3:1) are randomly located and part of them are on the surface of the microgel; (b) distribution $N(q_{\rm ch})$ of the number of charges per chain ($q_{\rm ch}$) for surface and randomly charged microgels.

chains, could be also the reason for which the most charged experimental sample analysed ($I_{\rm KPS} = 8.0\%$) shows a more compact structure at low temperatures (see Fig. 1(c)), while in simulations R_g/R_H decreases by increasing f. At the same time, we correctly observe for this sample that the minimum broadens by increasing charge content, as observed in simulations. Finally, the results in Fig. 5 allow us to exclude the presence of a minimum in R_g/R_H for highly cross-linked charged microgels. It would be interesting to test these predictions in experiments, for which, to our knowledge, no data for R_g/R_H are yet available for ionic microgels.

Varying the charge distribution

We have previously shown that the minimum also arises in randomly-charged microgels above a certain charge fraction for each considered c. This indicates that a fundamental role is played by charges located on the corona, where the screening action of counterions is lower than in the core of the particles. Moreover, the dependence of the minimum on c could be interpreted as a sign of the fact that the average length of polymer chains, being determined by c for a fixed number of monomers, plays its own role, too. Intuitively, we expect that on the surface, where chains interact less among each other with respect to the core, charge correlations along the same chain would act against chain collapse, resulting in the observed retarded deswelling. This viewpoint could suggest that if only one (uncorrelated) charge per chain was present, a minimum will not be observed even in surface-charged microgels. With this picture in mind, we now aim to determine and possibly quantify whether a minimum amount of charges per chain exists for the onset of the minimum in R_g/R_H.

To test the validity of these assumptions, we perform additional simulations for the $c = 5\%$ microgel with surface charges in which we vary *ad hoc* the charge distribution. While in Fig. 2 we focused on a surface charge distribution in which the charges are located at random on the surface monomers, we now analyse the swelling behaviour of microgels where charges are still located on the surface but with the additional constraint that a fixed number of charges per (surface) chain should be present, varying this number from one to three.

The behaviour of R_g/R_H for these cases is reported in Fig. 6(a). We clearly find confirmation that there is no minimum when only one charge per chain is present, even if they are all located on the surface (as shown by the charged monomers radial distributions in Fig. S6). A tiny minimum starts to appear when two charges per surface chain are present and finally a well-defined minimum occurs for three charges per chain. The systematic increase of the number of charges per surface chain makes the behaviour of R_g/R_H more and more similar to the originally considered case of surface charges that are randomly distributed throughout the corona, thus mimicking the experimental situation of pNIPAM with a given amount of initiator arranged on the outer part of the microgel surface in a disordered fashion. Not only the minimum becomes more pronounced, but its position also moves towards larger effective temperatures.

These trends are confirmed by increasing the charge content to $f = 10\%$, also shown in Fig. 6(a), for which we do

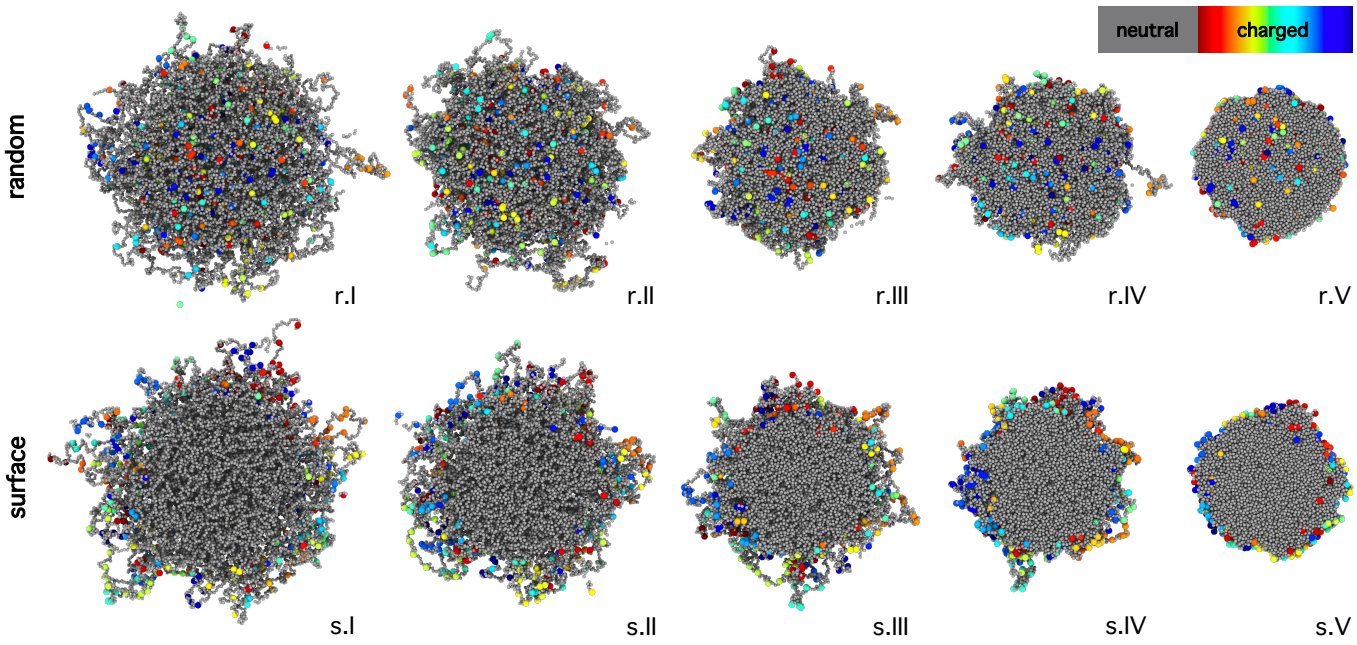

FIG. 7. **Snapshots highlighting charged beads.** Simulation snapshots representing slices of microgels with $f = 3.2\%$ and $c = 5\%$ with random (top row) and surface (bottom row) charge distribution referring to different values of the swelling parameter $\alpha = 0, 0.48, 0.74, 0.80, 1.20$ from the swollen to the collapsed state (from left to right). Charges belonging to the same chain are shown with the same color and enhanced size, to improve their visualisation, while uncharged monomers are grey.

not observe a total collapse of the microgel at high α (see Fig. S7), but still we find a rather deep miminum for $\alpha \sim 1.0$. Such a minimum appears to be wider with respect to that occurring at low f values, but the total hindering of the collapse indicates that probably such surface-charged microgel is not realizable in the experiments, given the high charge content. Hence, in addition, we analysed mixed charge distributions with $f = 10\%$, where different amount of charges were located at random and on the surface, respectively, also reported in Fig. 6(a). These systems display an intermediate behaviour between the random and the surface charged ones.

It is important to notice that, in the case of standard surface charge distribution with $f = 3.2\%$ discussed above, the average charge per surface chain is roughly equal to $\sim -1.4e^*$ only. However, the minimum is much more pronounced in this case than when the charge is set to be $-3e^*$. In this case, the variance of the number of charges per chain is not negligible, as displayed in Fig. 6(b). In this plot, we report the distribution of the number of charges per chain for random and surface charges with varying c and f, showing that all curves referring to microgels not displaying the two-step collapse are rather well-described by a single exponential decay, while those with a well-developed minimum reveal the onset of a tail in the distribution. This suggests the development of a characteristic correlation between charges on long chains, which makes the heterogeneous deswelling mechanism much more efficient. The standard deviation of the distribution of charges per chain is further enhanced at $c = 1.25\%$, due to the underlying network topology, making the minimum in R_g/R_H always more pronounced for low-crosslinked microgels than for the corresponding ones at higher c.

To visualize what happens at the level of single chains, we show in Fig. 7 the snapshots of a slice of a microgel for different values of α. In particular, we compare random and surface charge distributions with $f = 3.2\%$ and $c = 5.0\%$, and we draw with the same color charges belonging to the same chain. In this way, we aim to visualize the presence of multiple charges per chain and how the deswelling process is affected. We see that for randomly-charged microgels the charged chains, despite a few isolated cases, play a minor role in the overall collapse of the network, probably because they are rare and pulled by the neighboring neutral monomers towards the collapsed network with increasing α. Instead, for surface charged microgels, there are many more charged chains, each in turn with several charged monomers which prevent the chains from a full collapse. These microgels are thus found to maintain an extended conformation up to large values of α, even beyond the VPT. Hence, prior to the final collapse at very large α, the microgel clearly looks like an inner compact sphere decorated by many non-compact chains (see, for instance, Fig. 7(s.IV)).

Predicting the two-step collapse: a simple indicator

To take full advantage of the predictive ability of the simulations, we are now in the position to establish an indicator that may be useful in predicting the appearance of the minimum in R_g/R_H. Since we demonstrated that the two-step

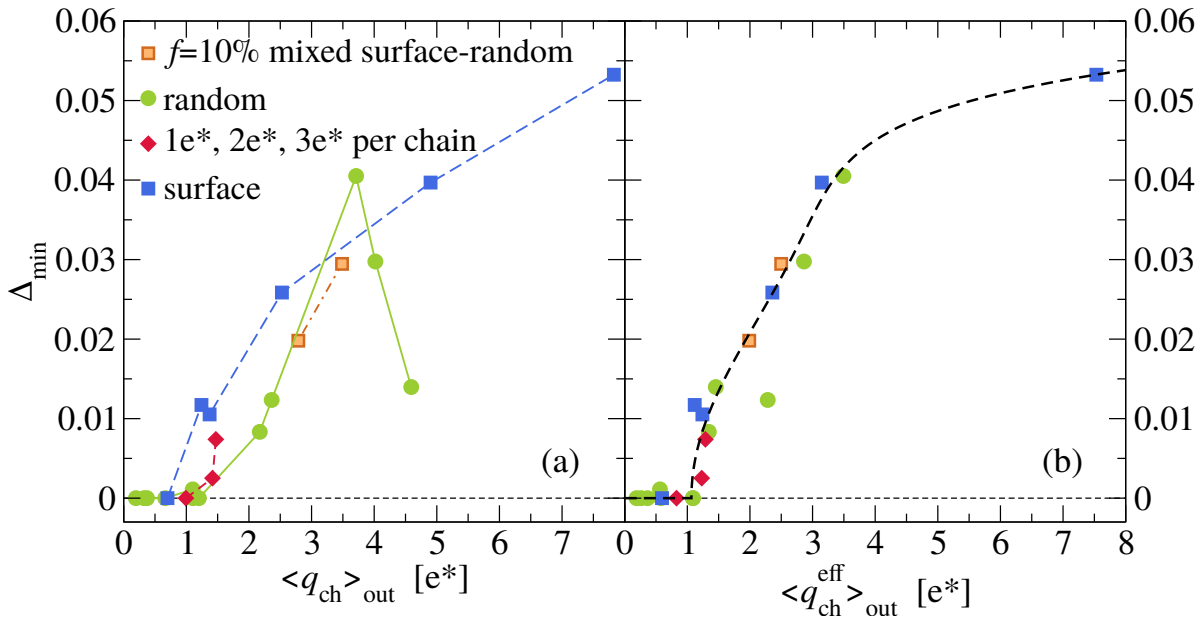

FIG. 8. **Prediction of two-step collapse.** Depth of the minimum $\Delta_{\min}$ as a function of the average charge of the surface chains, considering (a) bare $\langle q_{\rm ch}\rangle_{\rm out}$ or (b) effective charge $\langle q^{\rm eff}_{\rm ch}\rangle_{\rm out}$. The choice of the latter gives rise to a master plot that is followed by all simulated charged microgels, independently of crosslinker concentration, charge content and charge distribution. Lines are guides to the eye.

collapse is due to the explicit presence of charged groups in the microgels and preferentially to their arrangement on the microgel corona, we propose to identify the average number of charges per chain on the microgel surface, defined as $\langle q_{\rm ch}\rangle_{\rm out}$ as the observable that controls the onset and the development of the minimum. To verify that this is the case, we plot the dependence of the minimum depth $\Delta_{\min}$ as a function of $\langle q_{\rm ch}\rangle_{\rm out}$ in Fig. 8(a). We find that microgels with the same charge distribution, either surface or random, independently of their values of c and f, display characteristic behaviours that are roughly monotonic in $\langle q_{\rm ch}\rangle_{\rm out}$, except when this is very large in the case of randomly charged microgels (see below). We also notice that no minimum is observed when $\langle q_{\rm ch}\rangle_{\rm out} \lesssim 1$, meaning that on average more than one charge per surface chain is needed in order to develop the onset of the two-step collapse. Then, as $\langle q_{\rm ch}\rangle_{\rm out}$ increases, the depth of the minimum gets more and more pronounced both for surface-charged microgels and for those where we impose a fixed number of charges per chain. A similar behaviour is observed for microgels with random charges at low f content, and thus low $\langle q_{\rm ch}\rangle_{\rm out}$. However, when this increases, we find first a sudden growth of $\Delta_{\min}$, which even exceeds that of surface-charged microgels at the same $\langle q_{\rm ch}\rangle_{\rm out}$, followed by a drastic reduction and a highly non-monotonic behaviour, calling for a further refining of the chosen indicator.

To this aim, we exploit the explicit charge treatment in our simulations and consider the screening effect of the counterions, so that rather than the bare charge, we consider an effective charge per surface chain $\langle q^{\rm eff}_{\rm ch}\rangle_{\rm out}$ (see Methods and Fig. S10). Therefore, in Fig. 8(b) we plot the minimum depth $\Delta_{\min}$ as a function of $\langle q^{\rm eff}_{\rm ch}\rangle_{\rm out}$. Remarkably, a master plot is found where data for all simulated microgels (24 different systems in total) fall on the same curve manifesting the same behaviour. We notice that a couple of points are found to slightly deviate from the master curve, which may well be attributed to the statistical uncertainty of our calculations, which are carried out for a single topology and charge realization for each microgel. However, it is noteworthy that the use of the effective charge is able to completely remove the non-monotonicity of the data for randomly charged microgels as a function of bare charge, indicating the correctness of our procedure at least on a qualitative basis. In this respect, we remark that this is due to the fact that screening effects are much more effective for random rather than for surface charged microgels, which can be intuitively understood in terms of an overall reduced electrostatic repulsion experienced by the counterions when charges are distributed throughout the entire network, thus facilitating the microgel collapse.

DISCUSSION

In this work, we thoroughly investigated the swelling behaviour of microgels across the VPT upon varying crosslinker concentration and charge distribution. The study was motivated by experimental measurements of gyration and hydrodynamic radii that showed the appearance of a characteristic minimum in the ratio R_g/R_H at a temperature close to the VPT one. Such a minimum indicates that a different rate of collapse with increasing temperature takes place between the inner mass of the microgel, quantified in size by the gyration radius, and its outer mass, associated to the hydrodynamic radius. A similar evidence was also reported in few previous works[48,49], but its microscopic origin was not investigated in

detail so far. The new measurements reported in this paper for four different samples unambiguously reveal the presence of such a minimum. In a previous experimental work by some of us[50], the minimum was tentatively associated to the presence of initiator charges, manifesting their effect under collapsed conditions even for simple pNIPAM microgels. This conjecture was supported by electrophoretic mobility measurements also displaying a rapid increase of the signal for temperatures above the VPT, thus providing evidence that, in the high temperature regime, pNIPAM microgels have to be considered as charged micro-objects[34,53,56]. However, a legitimate doubt concerned whether the minimum in R_g/R_H would be solely due to charges or could be attributed to other ingredients, such as the inhomogeneous core-corona topology of pNIPAM microgels synthesized by precipitation polymerisation methods. For these reasons, the primary purpose of the present work was to correctly assess the role of charges on the occurrence of the minimum.

We thus performed an extensive set of simulations for several realistic microgels, with different crosslinker concentration, charge content and distribution. First of all, we found that the minimum does not occur for purely neutral microgels, even for very low cross-linked concentrations (like $c = 1.25\%$, the lowest value investigated in this work), where the inhomogeneous internal structure of the microgels is enhanced. Hence, we can safely exclude that the two-step collapse is associated to the topology, whereas it must be attributed to additional interactions emerging at the VPT which modify the homogeneous deswelling that would take place in a perfectly neutral microgel. Incidentally, it is important to notice that, to our knowledge, it is currently not possible to synthesize strictly uncharged microgels made of pNIPAM, the only example being for microgels made of (non-thermoresponsive) polystyrene[57], thus preventing confirmation of the present numerical predictions. Alternatively, experiments could be performed in the presence of added salt that would screen electrostatic interactions[56], though at the same time favoring microgel-microgel aggregation at high temperatures.

The additional mechanism giving rise to the two-step deswelling is thus attributed to electrostatic effects. In particular, charged initiator groups present within the network interact with the solvent in a different way with respect to NIPAM monomers as temperature increases, since they always maintain a solvophilic character, thus acting against collapse. When the amount of initiator is very low as in common synthesis procedures, these effects can be very subtle and may well depend on the location of these charges. Therefore, it is important to discriminate between random location of charges throughout the network and surface arrangement at the periphery of the corona. Indeed, the latter case seems to be appropriate to model charged initiators which start the polymerisation process and then possibly remain confined in the outer part of the microgel to minimize mutual electrostatic interactions. In this way, being localized on the surface, upon particle collapse the charged groups would start to strongly feel a mutual repulsion, thus influencing more strongly the corona deswelling as demonstrated in the previous sections. On the other hand, a random distribution of charges would 'dilute' the effect of the electrostatic contribution throughout the whole particle including the core, unlikely affecting the collapse of the particle during the VPT. The latter situation would thus be more appropriate to describe co-polymerised pNIPAM microgels, in the presence of a second component with ionic character such as PAAc.

The present simulation results clearly show that, for the typical amounts of initiators used in synthesis of pure pNIPAM microgels ($f = 3.2\%$) and standard crosslinker concentration (c=5%), a random distribution of charges does not give rise to a minimum in R_g/R_H, while this is present when charges are distributed only on the surface. Actually, the minimum for random charge arrangement only manifests at much higher f or lower c, a numerical prediction that awaits for experimental confirmation. Indeed, no measurements of R_g/R_H are currently available in the literature for ionic microgels and it would be important to clarify this point in the near future. Instead, we have shown that microgels with surface charge distribution are the appropriate model to describe the occurrence of the minimum in pNIPAM microgels, in agreement with experimental measurements and with previous hypothesis[46,52,58].

Another important point to be addressed in the future is to systematically vary the amount of initiator as well as the crosslinker concentration. The former parameter is relatively unexplored and it will be interesting to see to which extent it can be exploited, given that too large amount of initiator could give rise to synthesis by-products that would not necessarily be part of the microgel network. In addition, it could be possible that above some threshold, the charges would start to penetrate in the interior of the microgel giving rise to 'mixed' surface-random distribution, as discussed in Ref.[51]. Indeed, looking at the experimental behavior for I_{KPS}=8% (Fig. 1), we observe that this sample displays larger values of R_g/R_H at low temperatures and a shallower minimum at the VPT, in qualitative agreement with the effect of mixed charge distributions shown for the numerical data in Fig. 6. These findings seem to suggest that increasing the initiator molar fraction in the synthesis does not simply give rise to an augmented charge distribution peaked at the microgel periphery, but presumably homogenizes the initiator (and possibly the mass) distribution radially within the microgel. That said, a systematic experimental study of microgels with large differences of initiator fraction is needed to further substantiate this conjecture. Concerning the crosslinker concentration, we expect that for low c values microgels possess an extended corona with long dangling chains decorated with charged initiators, favoring the onset of a more pronounced minimum in R_g/R_H. On the contrary, for larger and larger c, it is likely that charged groups will permeate the inner structure, giving rise to mixed distributions for which the depth of the minimum could saturate and tend towards the behaviour observed for randomly charged (or ionic) microgels.

The numerical results of the present work will provide a framework to interpret data thanks to the master curve reported in Fig. 8, where we have been able to rationalize the behaviour of R_g/R_H for all different microgels within a single description. This was possible thanks to the use of a proper

indicator that is able to quantify the two-step deswelling process, i.e. the screened average charge per surface chain $\langle q_{\rm ch}^{\rm eff}\rangle_{\rm out}$. Unfortunately, at present, it appears difficult to estimate such an effective charge in experiments. However, it is important to notice that in experimental realizations of pNIPAM microgels, the charged initiator molecule should be predominantly found at a chain end, since a NIPAM monomer can in general form only one additional bond, after it is bound to the initiator. Nevertheless, at first sight our numerical findings, indicating that multiple charges per chain are needed in order to reproduce a two-step collapse, could seem not to be fully compatible with experiments, where chains carry at most one charge. To reconcile the two, a possible explanation could be based on the fact that crosslinkers and initiators are more chemically reactive than NIPAM[59], hence in the first stages of the synthesis one or two very short chains, each with a monovalent charge, could bind to a crosslinker, which in turn could be successively incorporated in a longer chain, effectively having more than one charged unit. Also, the difference in the reaction rates of the compounds may lead to a clustering of charges resulting in inhomogeneous distributions. Indeed, charge correlations among neighbour chains would have a similar effect on the swelling behavior as multiple charges per chain, giving rise to so-called nano-domains, which were experimentally observed to act against deswelling in recent high-speed Atomic Force Microscopy measurements[60], but not directly related to charged groups. In this respect, future works aimed to assess in a more quantitative way the distribution and local arrangement of charges should be actively performed. In particular, super-resolution or confocal microscopy experiments[61] could be helpful when combined with selective labeling of the surface or even of the initiators, as well as studies where the average bare charge and screening electrostatic conditions of the polymer chains would be systematically varied, as recently done in Ref.[62]. Finally, also neutron scattering measurements, where differentiations of the molecular components could be achieved by contrast variation[44,63,64], would be very valuable.

In the end, the outcomes of this work will also be relevant for the study of effective interactions and of the collective behaviour of pNIPAM microgels at high temperatures, where numerical/theoretical works are currently lacking. While it is now established that the effective potential for swollen conditions can be described by a soft repulsion, which builds on the Hertzian model[21,65], at high temperatures attractive interactions should become important[58,66], being mediated by the electrostatic interactions of the initiator. It will be therefore also necessary to assess whether these will contribute in a significant way to the collective and rheological behaviour of dense microgel suspensions.

MODELS, MATERIALS AND METHODS

Synthesis

Surfactant-free radical polymerisation has been used to synthesize poly-N-isopropyl-acrylamide (pNIPAM) microgels. Different batches have been prepared, varying the properties of the initiator, in order to obtain particles with different charge content. Specifically, we used methylene-bis-acrylamide (BIS) as crosslinker agent and two cationic initiators: potassium persulfate ($K_2S_2O_8$, KPS) and ammonium persulfate ($(NH_4)_2S_2O_8$, APS). Three different batches with $c = 5.25$mol% of BIS have been synthesized with the following initiator content and type: 1.6%mol of KPS; 1.6%mol of APS; 8.0%mol of KPS. Since our main focus is to scrutinize the role of initiator charges, we primarily use microgels obtained via surfactant-free emulsion polymerization, which allows us to minimize the impact of residual ionic surfactants on microgel deswelling. However, we also carried out one synthesis in the presence of surfactant and used the sample after purification. This allowed us to test the possible impact of surfactant addition, while at the same time reducing both the microgel size for low crosslinker content and the associated error on the R_g measurement. In this way, we obtained a batch of smaller particles, which has been prepared through the addition of an amount of 0.85mol% of sodium dodecyl-sulfate (SDS). In this case microgels are synthesized with $c = 1.37$mol% of BIS and 1.6mol% of KPS. All samples have been further purified through 3 consecutive cycles of centrifugation and supernatant replacement with deionized water. Finally, 2 mmol of sodium azide NaN_3 have been added to the final samples to prevent bacterial growth.

Experiments

To characterize the structure of particles in suspension we employed static and dynamic light scattering (SLS, DLS). For all the samples an aliquot of the mother batches (1wt% of NIPAM) has been diluted 60 times so to reach a mass fraction of 0.017wt% of NIPAM, equvalent to microgel volume fractions lower than 0.4% as determined by viscosimetry following the method detailed in Ref.[67]. All the scattering experiments have been performed by using the same laser source ($\lambda = 532$nm). Before each data acquisition, each sample has been thermostatted for 20min via a recirculating bath with 0.1°C accuracy and light has been collected by varying the scattering angle for SLS measurements with 1° accuracy. We extracted the average gyration radius of microgels, fitting the low scattering-vector part of the intensity $I(q)$ with the functional form (Guinier approximation):

$$I(q) = I(0)e^{-\frac{(qR_g)^2}{3}} \tag{1}$$

where $I(0)$ is a constant depending on the number of particles in the scattering volume and on the scattering factor of a single particle[68], while R_g is their radius of gyration, defined as:

$$R_g = \sqrt{\frac{\sum_{i=1}^{N}(\vec{r}_i - \vec{r}_{\rm cm})^2}{N}} \tag{2}$$

and q is the magnitude of the scattering vector. The Guinier approximation provides estimates for R_g with deviations not exceeding 30% for isotropic particles and a fitting range such that $qR_g < 2$[69]. Such uncertainty must be taken into account when the microgels synthesized in the absence of surfactant are in the swollen state, although Eq. 1 reliably fitted the available data in the entire range

$5.5\mu m^{-1} \leq q \leq 2/R_g$. For collapsed microgels, data could be robustly fitted by Eq. 1 in a q-range such that $qR_g < 1$ and the uncertainty is just given by the fit error, the latter being less than 10% of the best-fit value of R_g. For all the samples, $I(q)$ has been measured over a range of scattering wave-vectors going from $q = 5.55\mu m^{-1}$ to $q = 30\mu m^{-1}$.

Through dynamic light scattering we measured the autocorrelation function of the scattered intensity at a fixed value of $q = q_{\rm DLS}$. At high dilution conditions (non-interacting particles limit and gaussian approximation) this can be put in relation with the square of the self intermediate scattering function $F_s(\vec{q},t)^2$, which for simply diffusive systems has the functional shape of a convolution of exponential decays, taking into account the effects of polydispersity. The analysis of $F_s(\vec{q},t)^2$ has been performed by cumulant analysis, up to the second central moment of the distribution of decay rates:

$$F_s(\vec{q}_{\rm DLS},t)^2 \propto e^{-2q_{\rm DLS}^2 \bar{D} t} \left(1 + \frac{\mu_2 t^2}{2!} + o(t^3)\right)^2 \qquad (3)$$

where $\bar{D}$ is the average self-diffusion coefficient and μ_2 is related to the second moment of the distribution of D of the molecules in the sample. Using Stokes formula we obtain the average hydrodynamic radius as $R_H = k_B T/(6\pi\eta_0 \bar{D})$, and the corresponding dispersion is $\sigma_{R_H} = \sqrt{\mu_2} R_H/(\bar{D} q_{\rm DLS}^2)$, where k_B is the Boltzmann's constant, T the bath temperature and η_0 is the zero-shear viscosity of the solvent. For microgels with $c = 1.37\%$ we measured the intensity time-correlation function at $q_{\rm DLS} = 22\mu m^{-1}$, corresponding to an angle of 90°, while for microgels with $c = 5.25\%$ we gathered data at both $q_{\rm DLS} = 22\mu m^{-1}$ and $q_{\rm DLS} = 15.7\mu m^{-1}$ (the latter corresponding to an angle of 60°) in order to possibly detect and reject spurious effects of polydispersity when $q_{\rm DLS}$ was close to a value correspondent to the first minimum of the microgel form factor.

Some selected plots of the form factors with the Guinier fits and of the autocorrelation functions of the scattered intensity with the respective fits through Eq. 3 are shown in Fig. S8. The polydispersity indexes of the samples PDI $= \mu_2/(\bar{D} q_{\rm DLS}^2)$, calculated at $T \simeq 25$°C, are: (i) 0.065 for the microgels with $c = 1.37$mol% and $I_{\rm KPS} = 1.6$mol%, (ii) 0.148 for the microgels with $c = 5.25$mol% and $I_{\rm KPS} = 8.0$mol%, (iii) 0.074 for the microgels with $c = 5.25$mol% and $I_{\rm KPS} = 1.6$mol%, and (iv) 0.005 for the microgels with $c = 5.25$mol% and $I_{\rm APS} = 1.6$mol%.

Numerical simulations

We simulate single monomer-resolved microgels exploiting a recently developed protocol[35] that is able to generate fully-bonded, disordered polymer networks. By appropriately tuning the internal polymer distribution, the model faithfully reproduces measured swelling properties and form factors of neutral microgels across the VPT[15]. The resulting network structure is made of equal-size beads, representing polymer segments with their hydration shells of dimensions comparable to the Kuhn length, interacting with the well-established Kremer-Grest potential[70]. In this model, all beads experience a steric repulsion, modeled with the Weeks-Chandler-Anderson (WCA) potential:

$$V_{\rm WCA}(r) = \begin{cases} 4\varepsilon\left[\left(\frac{\sigma}{r}\right)^{12} - \left(\frac{\sigma}{r}\right)^{6}\right] + \varepsilon & \text{if} \quad r \leq 2^{1/6}\sigma \\ 0 & \text{if} \quad r > 2^{1/6}\sigma \end{cases} \qquad (4)$$

where ε and σ are respectively the energy and length units. In addition, connected beads also interact via the finitely extensible nonlinear elastic potential (FENE):

$$V_{\rm FENE}(r) = -\varepsilon k_F {R_0}^2 \log\left[1 - \left(\frac{r}{R_0\sigma}\right)^2\right], \quad r < R_0\sigma \qquad (5)$$

where $R_0 = 1.5\sigma$ is the maximum bond distance and $k_F = 15$ is a stiffness parameter influencing the rigidity of the bond. These bonds cannot break during the simulation, mimicking strong covalent bonding. Beads that are linked via FENE to two neighbours represent NIPAM monomers, while those mimicking crosslinkers have fourfold valence. We analyse in detail values of the crosslinker fraction similar to the experimental ones, i.e. c =1.25% and 5.0%. In order to be more quantitative on the c-dependence of results, we also provide specific additional results for $c = 3.0\%$, 7.5% and 10%.

We then consider that microgels obtained via free-radical polymerisation embed a certain amount of ionic groups in their backbone, in this case SO_4^-, which result from the dissociation of APS/KPS after a further thermal splitting of the ions $S_2O_8^{2-}$, starting the reaction and remaining attached to the network. We model electrostatics providing a fraction f of the beads with a negative charge and inserting an equivalent number of counterions with positive charge to preserve the overall electro-neutrality. Counterions interact sterically among each other and with microgel beads through the WCA potential. Their diameter is set to $\sigma_c = 0.1\sigma$ to avoid spurious effects from excluded volume in the collapsed state[37], while electrostatic interactions are given by the Coulomb potential, here expressed in reduced units:

$$V_{\rm coul}(r_{ij}) = \frac{q_i q_j \sigma}{{e^*}^2 r_{ij}}\varepsilon. \qquad (6)$$

where q_i and q_j are the charges of the beads, and $e^* = \sqrt{4\pi\varepsilon_0\varepsilon_r\sigma\varepsilon}$ is the reduced unit for the charge, embedding the vacuum and relative dielectric constants, ε_0 and ε_r. q_i and q_j are set to the values $-e^*$ or $+e^*$ whether it refers to charged beads or counterions. For different values of c we consider several values for the fraction of charged monomers, namely $f = 1.0\%, 2.0\%, 3.2\%, 10\%$ and 20%, as well as neutral microgels ($f = 0$). We analyse in detail the case $f = 3.2\%$, corresponding to an initiator concentration $I_{\rm KPS} = 1.6$%mol, that matches the nominal charge content of some of the experiments performed. Finally, we also consider $f = 10\%$, which is a relatively high charge fraction that should mimic the experimental situation with a nominal initiator content of $I_X = 8.0$%mol, assuming that in a synthesis process with a large quantity of highly reactive initiator radicals, a non-negligible amount of charged groups would end up in low molecular mass byproducts, that will be removed by filtration at the end of the process. For comparison, we also studied the neutral case, i.e. $f = 0$, in order to highlight effects entirely attributable to charges.

In our simulations the solvent is implicitly taken into account through an effective potential which mimics the gradual change in the affinity of the polymer for the solvent by raising temperature:

$$V_\alpha(r) = \begin{cases} -\varepsilon\alpha & \text{if } r \leq 2^{1/6}\sigma \\ \frac{1}{2}\alpha\varepsilon\left\{\cos\left[\gamma\left(\frac{r}{\sigma}\right)^2 + \beta\right] - 1\right\} & \text{if } 2^{1/6}\sigma < r \leq R_0\sigma \\ 0 & \text{if } r > R_0\sigma \end{cases} \qquad (7)$$

where α is the solvophobicity parameter representing the effective temperature, which is varied from $\alpha = 0$ (good solvent conditions) to $\alpha \gtrsim 1.40$ (bad solvent conditions) to reproduce the swelling curve from the swollen state to the most collapsed ones. $\gamma = \pi\left(\frac{9}{4} - 2^{1/3}\right)^{-1}$ and $\beta = 2\pi - \frac{9}{4}\gamma$ are constants defining the functional shape of the potential[71]. We showed in a previous work[38] that, for a correct description of charge effects, only neutral monomers

should interact with the additional V_α potential. Instead, charged monomers retain a solvophilic character at all temperatures, i.e. for the interaction among charged beads and other charged or neutral ones we always set $\alpha = 0$.

The thermodynamic temperature in simulations is set to $k_BT/\varepsilon = 1.0$ for all the runs. The equations of motion are integrated through a Nosé-Hoover thermostat in the constant NVT ensemble for the equilibration, and through a Velocity-Verlet algorithm in the constant-energy ensemble for the production runs, with an integration time-step $\Delta t = 0.002\tau$, where $\tau = \sqrt{m\sigma^2/\varepsilon}$ is the reduced time unit. All simulations are performed with the LAMMPS package[72].

For all the simulations we consider microgels consisting of $N \sim 42000$ monomer beads, synthesized in a spherical cavity of radius $Z = 50\sigma$[15]. For all the studied values of f we analysed a random charge distribution, with charged beads randomly distributed throughout the network (except on crosslinkers), and for some f values we also studied a surface distribution, with charged beads distributed only onto the surface chains. To this aim, starting from an equilibrated neutral configuration, either we randomly pick up a bead and assign it a charge $-1e$ until the overall charged fraction reaches the desired value (random distribution) or we randomly choose the beads in the exterior corona only, such that $\vec{r}_i - \vec{r}_{cm} > R_g$ (where $\vec{r}_{cm}$ is the centre of mass of the microgel). In few cases we also analysed other distributions, such as mixed distributions, where part of the monomers is distributed randomly throughout the network and the remaining according to the foregoing procedure. We also considered surface chain distributions, where we assigned a fixed number of charges to each chain starting from those whose centre-of-mass distance from the microgel's centre is greater.

Long-range Coulomb interactions are computed with the particle-particle-particle-mesh method[73]. The equilibration of each system is carried out for 2000τ. Subsequently, a longer production run of 6000τ from which we extracted the equilibrium averages of the main observables of interest, such as the gyration radius R_g and the density profile, defined as the average density at a fixed distance from the centre of mass:

$$\rho_s(r) = \left\langle \frac{\sum_{i=1}^{N_s} \delta(|\vec{r}_i - \vec{r}_{\rm cm}| - r)}{N_s} \right\rangle. \tag{8}$$

Here, the subscript s indicates the species of particles considered.

We notice that the calculation of the hydrodynamic radius in simulations is not straightforward as that of the radius of gyration. Indeed, a proper estimate of R_H would require the knowledge of the long-time dynamics of the microgel in the solvent, to extract its self-diffusion coefficient, which is currently beyond our computational capabilities for a realistic, monomer-resolved particle. To avoid this, we previously resorted to an operative definition of R_H, defined as the value where the monomer density profile assumes a given threshold value, e.g. $\rho_m(R^*) = 10^{-3}\sigma^{-3}$[15].

Here instead, we introduce a different way to define R_H, by which we instantaneously approximate the microgel to an effective ellipsoid[65] and then calculate the hydrodynamic friction using the approach developed by Hubbard and Douglas[74]. Specifically, for each instantaneous configuration, we first compute the convex hull containing all the beads of the microgel and then evaluate the gyration tensor of all the simplices it is made of. Finally, we determine the ellipsoid having the same gyration tensor as previously done in Ref.[65]. To compute the hydrodynamic friction ζ of each ellipsoid we exploited the relation[74]:

$$\zeta = 6\pi\eta C_\Omega \equiv 6\pi\eta R_H \tag{9}$$

where η is the solvent viscosity and C_Ω is the electrostatic capacitance. This relation has been shown to well approximate the friction acting on brownian rigid particles and to be valid for objects of arbitrary shape[41]. Eqn. 9 is based on a solution of the Navier-Stokes equation for steady flow of rigid particles with stick boundary conditions, where the hydrodynamic interactions are described by the isotropic angular averaged Oseen tensor[74]. In this approximation, the Navier-Stokes equation for the momentum flux density assumes the same form of the Poisson's equation for electrostatics, thereby the hydrodynamic radius becomes mathematically equivalent to the electrostatic capacitance, which for rigid ellipsoids is[74]:

$$C_\Omega = 2\left[\int_0^\infty \frac{1}{\sqrt{(a^2+\theta)(b^2+\theta)(c^2+\theta)}} d\theta\right]^{-1} \tag{10}$$

where a, b, c are the principal semiaxes.

In the SM, we compare different approaches to the calculation of R_H, showing that they all provide similar qualitative results for the onset of a minimum in R_g/R_H close to the VPT. However, the approach here described provides the most reliable results, also in terms of the limits of R_g/R_H in the fully swollen and fully collapsed configurations. We thus adopt such definition throughout the manuscript.

Finally, to evidence the differences in the local structure at different distances from the centre of mass of microgels, we also calculated the local swelling curve as the volume of three different regions, defined on the basis of the quantity of monomers they contain. Ordering the polymer beads according to their distance from the centre of mass, at each time we can associate the most inner fraction of monomers $f_{\rm m,I} = 0.65$ of beads to the core (region I), the subsequent fraction $f_{\rm m,II} = 0.20$ of them to the inner corona shell (region II), and the farthest fraction of $f_{\rm m,III} = 0.15$ beads to the outer corona shell (region III). We chose the fraction $f_{\rm m,I}$ in such a way that the core region show an overall constant density profile at all c and α values. Consequently, we picked up the values of $f_{\rm m,II}$ and $f_{\rm m,III}$ in such a way that the monomers density profile at the boundary separating the two corona shells takes a value close to half the average density of the core region, to separate the more crosslinked inner part of the corona from the most external region with low density dangling chains (see Fig. S2). In this way, we can well define boundary surfaces between the regions, since the beads do not have a fixed position in the polymeric network (they can pass by the boundary among two contiguous regions several times along a trajectory) and, most importantly, we can follow the collapse of all the three regions across the VPT without definition ambiguities. The volumes of the three concentric regions, and their outer surfaces, is calculated as the convex hull enclosing all the beads associated to them.

To quantify the distributions of charges per chain, we first of all calculate the chain length distribution, where each chain is defined as the sequence of monomers between two crosslinkers, except for dangling chains, which have only one crosslinker. We then count the number of charged monomers for each chain ($q_{\rm ch}$). To build the master plot in Fig. 8, we define the extent of the minimum $\Delta_{\rm min}$ as the difference between the value of R_g/R_H at $\alpha = 0.5$ and at its minimum. We notice that in the region $0 < \alpha \lesssim 0.5$, R_g/R_H is roughly constant, but we avoid to use as a reference the value of R_g/R_H at lower α values to avoid spurious effects not related to the VPT. In addition, we define the average number of charges per chain on the microgel surface, defined as $\langle q_{\rm ch}\rangle_{\rm out}$, where $q_{\rm ch}$ is averaged only over chains whose average centre of mass distance from the microgel's centre of mass is greater than R_g . To take into account screening effects by counterions, we also define the effective charge per surface chain $\langle q^{\rm eff}_{\rm ch}\rangle_{\rm out}$, that is obtained by considering for each charged monomer an average screened charge based on the integration of the ion-counterion pair-distribution function up to a determined distance, as discussed in the SM.

SUPPLEMENTARY MATERIALS

ACKNOWLEDGMENTS

We thank E. Buratti, E. Lattuada, J. Ruiz-Franco, P. Schurtenberger and F. Sciortino for valuable discussions. We acknowledge financial support from the European Research Council (ERC Consolidator Grant 681597, MIMIC), from the European Union's Horizon 2020 research and innovation programme (Grant 731019, EUSMI), from MIUR (FARE project R16XLE2X3L, SOFTART), and from the Agence Nationale de la Recherche (ANR) (Grant N° ANR-20-CE06-0030-01, THELECTRA). The authors gratefully acknowledge the computing time granted by EUSMI on the supercomputer JURECA at the Jülich Supercomputing Centre (JSC).

COMPETING INTERESTS

The authors declare that they have no competing interests.

[1] A. Fernandez-Nieves, H. Wyss, J. Mattsson, and D. A. Weitz, *Microgel suspensions: fundamentals and applications* (John Wiley & Sons, 2011).
[2] J. Lee, K. H. Ku, M. Kim, J. M. Shin, J. Han, C. H. Park, G.-R. Yi, S. G. Jang, and B. J. Kim, "Stimuli-responsive, shape-transforming nanostructured particles," Advanced materials **29**, 1700608 (2017).
[3] C. Lanz, M. Schlötter, N. Klinkenberg, P. Besirske, and S. Polarz, "Stimuli-responsive particle-based amphiphiles as active colloids prepared by anisotropic click chemistry," Angewandte Chemie International Edition **59**, 8902–8906 (2020).
[4] A. M. Mihut, B. Stenqvist, M. Lund, P. Schurtenberger, and J. J. Crassous, "Assembling oppositely charged lock and key responsive colloids: A mesoscale analog of adaptive chemistry," Science advances **3**, e1700321 (2017).
[5] S. Medeiros, A. Santos, H. Fessi, and A. Elaissari, "Stimuli-responsive magnetic particles for biomedical applications," International journal of pharmaceutics **403**, 139–161 (2011).
[6] J. F. Quinn, M. R. Whittaker, and T. P. Davis, "Glutathione responsive polymers and their application in drug delivery systems," Polymer Chemistry **8**, 97–126 (2017).
[7] A. M. Wagner, D. S. Spencer, and N. A. Peppas, "Advanced architectures in the design of responsive polymers for cancer nanomedicine," Journal of applied polymer science **135**, 46154 (2018).
[8] M. Wang, A. M. Mihut, E. Rieloff, A. P. Dabkowska, L. K. Månsson, J. N. Immink, E. Sparr, and J. J. Crassous, "Assembling responsive microgels at responsive lipid membranes," Proceedings of the National Academy of Sciences **116**, 5442–5450 (2019).
[9] S. Jia, Z. Tang, Y. Guan, and Y. Zhang, "Order–disorder transition in doped microgel colloidal crystals and its application for optical sensing," ACS applied materials & interfaces **10**, 14254–14258 (2018).
[10] L. Prodi, "Luminescent chemosensors: from molecules to nanoparticles," New journal of chemistry **29**, 20–31 (2005).
[11] D. S. Shin, E. Y. Tokuda, J. L. Leight, C. E. Miksch, T. E. Brown, and K. S. Anseth, "Synthesis of microgel sensors for spatial and temporal monitoring of protease activity," ACS biomaterials science & engineering **4**, 378–387 (2018).
[12] L. A. Lyon and A. Fernandez-Nieves, "The polymer/colloid duality of microgel suspensions," Annual review of physical chemistry **63**, 25–43 (2012).
[13] R. Pelton and T. Hoare, "Microgels and their synthesis: An introduction," Microgel Suspensions: Fundamentals and Applications **1**, 1–32 (2011).
[14] M. Stieger, W. Richtering, J. S. Pedersen, and P. Lindner, "Small-angle neutron scattering study of structural changes in temperature sensitive microgel colloids," The Journal of chemical physics **120**, 6197–6206 (2004).
[15] A. Ninarello, J. J. Crassous, D. Paloli, F. Camerin, N. Gnan, L. Rovigatti, P. Schurtenberger, and E. Zaccarelli, "Modeling microgels with a controlled structure across the volume phase transition," Macromolecules **52**, 7584–7592 (2019).
[16] S. Seiffert and D. A. Weitz, "Microfluidic fabrication of smart microgels from macromolecular precursors," Polymer **51**, 5883–5889 (2010).
[17] G. M. Conley, C. Zhang, P. Aebischer, J. L. Harden, and F. Scheffold, "Relationship between rheology and structure of interpenetrating, deforming and compressing microgels," Nature communications **10**, 2436 (2019).
[18] G. M. Conley, S. Nöjd, M. Braibanti, P. Schurtenberger, and F. Scheffold, "Superresolution microscopy of the volume phase transition of pnipam microgels," Colloids and Surfaces A: Physicochemical and Engineering Aspects **499**, 18–23 (2016).
[19] F. Scheffold, "Pathways and challenges towards a complete characterization of microgels," Nature Communications **11**, 1–13 (2020).
[20] S. Bergmann, O. Wrede, T. Huser, and T. Hellweg, "Super-resolution optical microscopy resolves network morphology of smart colloidal microgels," Physical Chemistry Chemical Physics **20**, 5074–5083 (2018).
[21] M. J. Bergman, N. Gnan, M. Obiols-Rabasa, J.-M. Meijer, L. Rovigatti, E. Zaccarelli, and P. Schurtenberger, "A new look at effective interactions between microgel particles," Nature communications **9**, 1–11 (2018).
[22] F. Camerin, N. Gnan, J. Ruiz-Franco, A. Ninarello, L. Rovigatti, and E. Zaccarelli, "Microgels at interfaces behave as 2d elastic particles featuring reentrant dynamics," Physical Review X **10**, 031012 (2020).
[23] M. Rey, M. A. Fernandez-Rodriguez, M. Karg, L. Isa, and N. Vogel, "Poly-n-isopropylacrylamide nanogels and microgels at fluid interfaces," Accounts of chemical research **53**, 414–424 (2020).
[24] M. A. Fernandez-Rodriguez, A. Martín-Molina, and J. Maldonado-Valderrama, "Microgels at interfaces, from mickering emulsions to flat interfaces and back," Advances in Colloid and Interface Science **288**, 102350 (2021).
[25] G. Agrawal and R. Agrawal, "Stimuli-responsive microgels and microgel-based systems: Advances in the exploitation of microgel colloidal properties and their interfacial activity," Polymers **10**, 418 (2018).
[26] S. Minami, D. Suzuki, and K. Urayama, "Rheological aspects of colloidal gels in thermoresponsive microgel suspensions: formation, structure, and linear and nonlinear viscoelasticity," Current Opinion in Colloid & Interface Science **43**, 113–124 (2019).
[27] P. J. Yunker, K. Chen, M. D. Gratale, M. A. Lohr, T. Still, and A. Yodh, "Physics in ordered and disordered colloidal matter composed of poly (n-

isopropylacrylamide) microgel particles," Reports on Progress in Physics **77**, 056601 (2014).
[28]K. A. Agbim and L. A. Schaefer, "Investigation of thermoresponsive microgel polymer swelling theory," Polymer Reviews **60**, 648–670 (2020).
[29]J. Brijitta and P. Schurtenberger, "Responsive hydrogel colloids: Structure, interactions, phase behaviour, and equilibrium and non-equilibrium transitions of microgel dispersions," Current Opinion in Colloid & Interface Science **40**, 87–103 (2019).
[30]M. Karg, A. Pich, T. Hellweg, T. Hoare, L. A. Lyon, J. Crassous, D. Suzuki, R. A. Gumerov, S. Schneider, I. I. Potemkin, *et al.*, "Nanogels and microgels: From model colloids to applications, recent developments, and future trends," Langmuir **35**, 6231–6255 (2019).
[31]A. Martín-Molina and M. Quesada-Pérez, "A review of coarse-grained simulations of nanogel and microgel particles," Journal of Molecular Liquids **280**, 374–381 (2019).
[32]L. Rovigatti, N. Gnan, L. Tavagnacco, A. J. Moreno, and E. Zaccarelli, "Numerical modelling of non-ionic microgels: an overview," Soft matter **15**, 1108–1119 (2019).
[33]J. Oberdisse and T. Hellweg, "Recent advances in stimuli-responsive core-shell microgel particles: synthesis, characterisation, and applications," Colloid and Polymer Science **298**, 921–935 (2020).
[34]A. Scotti, U. Gasser, E. S. Herman, M. Pelaez-Fernandez, J. Han, A. Menzel, L. A. Lyon, and A. Fernández-Nieves, "The role of ions in the self-healing behavior of soft particle suspensions," Proceedings of the National Academy of Sciences **113**, 5576–5581 (2016).
[35]N. Gnan, L. Rovigatti, M. Bergman, and E. Zaccarelli, "In silico synthesis of microgel particles," Macromolecules **50**, 8777–8786 (2017), https://doi.org/10.1021/acs.macromol.7b01600.
[36]F. Camerin, M. A. Fernandez-Rodriguez, L. Rovigatti, M.-N. Antonopoulou, N. Gnan, A. Ninarello, L. Isa, and E. Zaccarelli, "Microgels adsorbed at liquid–liquid interfaces: A joint numerical and experimental study," ACS nano **13**, 4548–4559 (2019).
[37]G. Del Monte, A. Ninarello, F. Camerin, L. Rovigatti, N. Gnan, and E. Zaccarelli, "Numerical insights on ionic microgels: structure and swelling behaviour," Soft matter **15**, 8113–8128 (2019).
[38]G. Del Monte, F. Camerin, A. Ninarello, N. Gnan, L. Rovigatti, and E. Zaccarelli, "Charge affinity and solvent effects in numerical simulations of ionic microgels," Journal of Physics: Condensed Matter **33**, 084001 (2020).
[39]K. Haydukivska, V. Blavatska, and J. Paturej, "Universal size ratios of gaussian polymers with complex architecture: radius of gyration vs hydrodynamic radius," Scientific Reports **10**, 1–11 (2020).
[40]C. M. Kok and A. Rudin, "Relationship between the hydrodynamic radius and the radius of gyration of a polymer in solution," Die Makromolekulare Chemie, Rapid Communications **2**, 655–659 (1981).
[41]J. F. Douglas, H.-X. Zhou, and J. B. Hubbard, "Hydrodynamic friction and the capacitance of arbitrarily shaped objects," Physical Review E **49**, 5319 (1994).
[42]J. Roovers and J. Martin, "The hard-sphere model for linear and regular star polybutadienes," Journal of Polymer Science Part B: Polymer Physics **27**, 2513–2524 (1989).
[43]H. Senff and W. Richtering, "Temperature sensitive microgel suspensions: Colloidal phase behavior and rheology of soft spheres," The Journal of chemical physics **111**, 1705–1711 (1999).
[44]S. Nöjd, P. Holmqvist, N. Boon, M. Obiols-Rabasa, P. S. Mohanty, R. Schweins, and P. Schurtenberger, "Deswelling behaviour of ionic microgel particles from low to ultra-high densities," Soft Matter **14**, 4150–4159 (2018).
[45]D. Capriles-González, B. Sierra-Martín, A. Fernández-Nieves, and A. Fernández-Barbero, "Coupled deswelling of multiresponse microgels," The Journal of Physical Chemistry B **112**, 12195–12200 (2008).
[46]J. Zhou, J. Wei, T. Ngai, L. Wang, D. Zhu, and J. Shen, "Correlation between dielectric/electric properties and cross-linking/charge density distributions of thermally sensitive spherical pnipam microgels," Macromolecules **45**, 6158–6167 (2012).
[47]O. Virtanen, A. Mourran, P. Pinard, and W. Richtering, "Persulfate initiated ultra-low cross-linked poly (n-isopropylacrylamide) microgels possess an unusual inverted cross-linking structure," Soft matter **12**, 3919–3928 (2016).
[48]L. Arleth, X. Xia, R. P. Hjelm, J. Wu, and Z. Hu, "Volume transition and internal structures of small poly (n-isopropylacrylamide) microgels," Journal of Polymer Science Part B: Polymer Physics **43**, 849–860 (2005).
[49]Y. Sun, "Investigation of volume phase transition from the different properties of particles," (2005), arXiv:physics/0511160, arXiv:physics/0511160.
[50]D. Truzzolillo, S. Sennato, S. Sarti, S. Casciardi, C. Bazzoni, and F. Bordi, "Overcharging and reentrant condensation of thermoresponsive ionic microgels," Soft Matter **14**, 4110–4125 (2018).
[51]C. Huang, H. Kobayashi, M. Moritaka, and M. Okubo, "Hollow particles are produced by the burying of sulfate end-groups inside particles prepared by emulsion polymerization of styrene with potassium persulfate as initiator in the absence/presence of a nonionic emulsifier," Polymer Chemistry **8**, 6972–6980 (2017).
[52]E. Daly and B. R. Saunders, "Temperature–dependent electrophoretic mobility and hydrodynamic radius measurements of poly (n-isopropylacrylamide) microgel particles: structural insights," Physical Chemistry Chemical Physics **2**, 3187–3193 (2000).
[53]S. Sennato, E. Chauveau, S. Casciardi, F. Bordi, and D. Truzzolillo, "The double-faced electrostatic behavior of pnipam microgels," (2021), arXiv:2103.09361.
[54]K. Kratz, T. Hellweg, and W. Eimer, "Influence of charge density on the swelling of colloidal poly (n-isopropylacrylamide-co-acrylic acid) microgels," Colloids and Surfaces A: Physicochemical and Engineering Aspects **170**, 137–149 (2000).
[55]D. Capriles-González, B. Sierra-Martín, A. Fernández-Nieves, and A. Fernández-Barbero, "Coupled deswelling of multiresponse microgels," The Journal of Physical Chemistry B **112**, 12195–12200 (2008).
[56]M. Braibanti, C. Haro-Pérez, M. Quesada-Pérez, L. F. Rojas-Ochoa, and V. Trappe, "Impact of volume transition on the net charge of poly-n-isopropyl acrylamide microgels," Physical Review E **94**, 032601 (2016).
[57]P. Van Der Scheer, T. Van De Laar, J. Van Der Gucht, D. Vlassopoulos, and J. Sprakel, "Fragility and strength in nanoparticle glasses," ACS nano **11**, 6755–6763 (2017).
[58]A. M. Howe, S. Desrousseaux, L. S. Lunel, J. Tavacoli, H. N. Yow, and A. F. Routh, "Anomalous viscosity jump during the volume phase transition of poly (n-isopropylacrylamide) particles," Advances in colloid and interface science **147**, 124–131 (2009).
[59]X. Wu, R. Pelton, A. Hamielec, D. Woods, and W. McPhee, "The kinetics of poly (n-isopropylacrylamide) microgel latex formation," Colloid and polymer science **272**, 467–477 (1994).
[60]Y. Nishizawa, S. Matsui, K. Urayama, T. Kureha, M. Shibayama, T. Uchihashi, and D. Suzuki, "Non-thermoresponsive decanano-sized domains in thermoresponsive hydrogel microspheres revealed by temperature-controlled high-speed atomic force microscopy," Angewandte Chemie International Edition **58**, 8809–8813 (2019).
[61]G. M. Conley, P. Aebischer, S. Nöjd, P. Schurtenberger, and F. Scheffold, "Jamming and overpacking fuzzy microgels: Deformation, interpenetration, and compression," Science advances **3**, e1700969 (2017).
[62]M. J. Bergman, J. S. Pedersen, P. Schurtenberger, and N. Boon, "Controlling the morphology of microgels by ionic stimuli," Soft matter **16**, 2786–2794 (2020).
[63]P. S. Mohanty, S. Nöjd, K. van Gruijthuijsen, J. J. Crassous, M. Obiols-Rabasa, R. Schweins, A. Stradner, and P. Schurtenberger, "Interpenetration of polymeric microgels at ultrahigh densities," Scientific Reports **7**, 1–12 (2017).
[64]A. Scotti, M. Brugnoni, A. Rudov, J. Houston, I. Potemkin, and W. Richtering, "Hollow microgels squeezed in overcrowded environments," The journal of chemical physics **148**, 174903 (2018).
[65]L. Rovigatti, N. Gnan, A. Ninarello, and E. Zaccarelli, "Connecting elasticity and effective interactions of neutral microgels: The validity of the hertzian model," Macromolecules **52**, 4895–4906 (2019).
[66]G. Chaudhary, A. Ghosh, J. G. Kang, P. V. Braun, R. H. Ewoldt, and K. S. Schweizer, "Linear and nonlinear viscoelasticity of concentrated thermoresponsive microgel suspensions," (2021), arXiv:2103.02108.
[67]D. Truzzolillo, V. Roger, C. Dupas, S. Mora, and L. Cipelletti, "Bulk and interfacial stresses in suspensions of soft and hard colloids," Journal of Physics: Condensed Matter **27**, 194103 (2015).
[68]G. Beaucage, "Approximations leading to a unified exponential/power-law approach to small-angle scattering," Journal of Applied Crystallography **28**, 717–728 (1995).
[69]L. Feigin and D. I. Svergun, *Structure analysis by small-angle X-ray and neutron scattering*, Vol. 1 (Springer, 1987).

[70]G. S. Grest and K. Kremer, "Molecular dynamics simulation for polymers in the presence of a heat bath," Physical Review A **33**, 3628 (1986).
[71]T. Soddemann, B. Dünweg, and K. Kremer, "A generic computer model for amphiphilic systems," The European Physical Journal E **6**, 409–419 (2001).
[72]S. Plimpton, "Fast parallel algorithms for short-range molecular dynamics," Journal of Computational Physics **117**, 1–19 (1995).
[73]M. Deserno and C. Holm, "How to mesh up ewald sums. i. a theoretical and numerical comparison of various particle mesh routines," The Journal of chemical physics **109**, 7678–7693 (1998).
[74]J. B. Hubbard and J. F. Douglas, "Hydrodynamic friction of arbitrarily shaped brownian particles," Physical Review E **47**, R2983 (1993).

Supplementary Materials for: Two-step deswelling in the Volume Phase Transition of thermoresponsive microgels

Giovanni Del Monte,[1,2,3] Domenico Truzzolillo,[4,a)] Fabrizio Camerin,[2,1] Andrea Ninarello,[2,1] Edouard Chauveau,[4] Letizia Tavagnacco,[2,1] Nicoletta Gnan,[2,1] Lorenzo Rovigatti,[1,2] Simona Sennato,[2,1] and Emanuela Zaccarelli[2,1,b)]

[1)]*Department of Physics, Sapienza University of Rome, p.le A. Moro 2 00185 Roma, Italy*

[2)]*CNR-ISC, Sapienza University of Rome, p.le A. Moro 2, 00185 Roma, Italy*

[3)]*CLNS, Istituto Italiano di Tecnologia, v.le Regina Elena 291, 00161 Roma, Italy*

[4)]*Laboratoire Charles Coulomb (L2C), UMR 5221 CNRS-Universitè de Montpellier, 4 F-34095 Montpellier, France*

(Dated: 22 April 2021)

[a)]domenico.truzzolillo@umontpellier.fr

[b)]emanuela.zaccarelli@cnr.it

Section 1. TRANSITION TEMPERATURES

Here we report the transition temperatures T_c of both R_g and R_H for the experimental samples, and the analogous effective temperatures α_c for the simulated microgels. For numerical data we simply calculate α_c as the inflection point of a spline fit of the data. In experiments it is more convenient to extract T_c from fits of the swelling curves through the phenomenological function

$$R(T) = R_0 - \Delta R \tanh\left[s(T-T_c)\right] + A(T-T_c) + B(T-T_c)^2 + C(T-T_c)^3 \tag{1}$$

that is able to accurately capture the behavior of both R_g and R_H in the whole investigated temperature range, avoiding spurious effects from the large fluctuations.

		Fits with Eq.1		Fit errors	
c [%mol]	I_X [%mol]	$T_c^{R_g}$ [°C]	$T_c^{R_H}$ [°C]	$\Delta T_c^{R_g}$ [°C]	$\Delta T_c^{R_H}$ [°C]
5.25	1.6 (KPS)	31.6	32.4	0.5	0.8
5.25	1.6 (APS)	30.9	32.1	1.1	3.4
5.25	8.0 (KPS)	33.3	33.7	0.4	2.4
1.37	1.6 (KPS)	30.9	31.3	0.3	1.8

TABLE S1: **Estimated values of the VPT temperature** T_c obtained through fits of the swelling curves for R_g and R_h with Eq. 1 (columns 3 and 4) and related errors (columns 5 and 6) for the different microgel samples. Here, c and I_X ($X = KPS, APS$) are the molar fractions used for, respectively, the crosslinker and the initiator during the synthesis.

We avoid to use the Flory-Rehner equation, that involves numerous (7) free parameters, and moreover it has been argued not to be able to quantitatively describe the experimental swelling of PNIPAM microgels[1]. In Tab. S1 the experimental transition temperatures for R_g and R_H are reported.

First of all we notice that the value of T_c is similar for all three samples with $c = 5.25\%$ of crosslinker, as expected. In addition, we find that the VPT temperature is slightly lower for R_g with respect to R_H by about $0.5 \div 1.0$°C. For the highly charged sample, with a nominal initiator concentration of $I_{KPS} = 8.0$mol%, we find a larger T_c for both R_g and R_H , in agreement with previous studies on charged microgels[2,3].

c [%]	f [%]	$\alpha_c^{R_g}$	$\alpha_c^{R_H}$
1.25	0	0.62	0.65
3.0	0	0.64	0.66
5.0	0	0.68	0.69
10.0	0	0.60	0.65

(a) neutral microgels.

c [%]	f [%]	$\alpha_c^{R_g}$	$\alpha_c^{R_H}$
1.25	1.0	0.66	0.69
3.0	1.0	0.63	0.69
5.0	1.0	0.66	0.68
1.25	2.0	0.70	0.77
1.25	3.2	0.76	0.78
3.0	3.2	0.73	0.82
5.0	3.2	0.69	0.75
10.0	3.2	0.69	0.72
3.0	10	0.89	1.04
5.0	10	0.79	1.04

(b) random charge distributions.

c [%]	f [%]	$\alpha_c^{R_g}$	$\alpha_c^{R_H}$
1.25	3.2	0.72	0.87
3.0	3.2	0.69	0.95
5.0	3.2	0.63	0.90
10.0	3.2	0.77	0.86
5.0	10	0.66	-

(c) surface charge distributions.

c [%]	$q*$ per chain $[-e*]$	$\alpha_c^{R_g}$	$\alpha_c^{R_H}$
5.0	1	0.72	0.72
5.0	2	0.68	0.78
5.0	3	0.68	0.87

(d) charges on surface chains ($f = 3.2\%$).

TABLE S2: **Estimated values of the solvophobic parameter α_c at the VPT** obtained through splined fits of the swelling curves for R_g and R_h for numerical microgels. Here, c and f are the crosslinker and the charged beads percentage, respectively. The fit error is negligible compared to the discretisation error, for which an upper limit can be quantified as $\Delta\alpha_c \sim 0.05$.

This scenario is in qualitative agreement with simulations data, for which the values of α_c are summarised in Table S2. Similarly to what observed in experiments, the value of α_c is found to depend on the amount of charges on the microgels, while the dependence on crosslinker concentration seems to be negligible. Indeed, for a given value of f, differences in the data are found to be within the error, considering this to be of the order of 0.05, given the used sampling of α. In particular, we find that it increases with increasing f and also moving from a random to a surface

distribution of the ionic monomers. Again, we also find that the estimated α_c is slightly larger when estimated from R_H than from R_g. We note that for a microgel with c=5% and f=10% arranged on the surface, a robust value of α_c could not be estimated because we did not detect the full collapse of the microgel.

Section 2. ELECTROPHORETIC MOBILITY

In Fig. S1 we show the T-dependence of the electrophoretic mobility $\mu_{\rm el}$ measured for three of the samples discussed in the manuscript. In agreement with previous works[4], we find that a strong increase of $\mu_{\rm el}$ is observed close to the VPT transition. In particular, we observe that c=5% microgels (squares and circles in Fig. S1) at low T have much lower values of $\mu_{\rm el}$ with respect to c=1.37% microgels (triangles in Fig. S1) at the same charge fraction. This may be due to the larger size of the former, since in the swollen state they have lower diffusivity and better screening conditions (lower surface-to-volume ratio). The transition temperature seems to increase

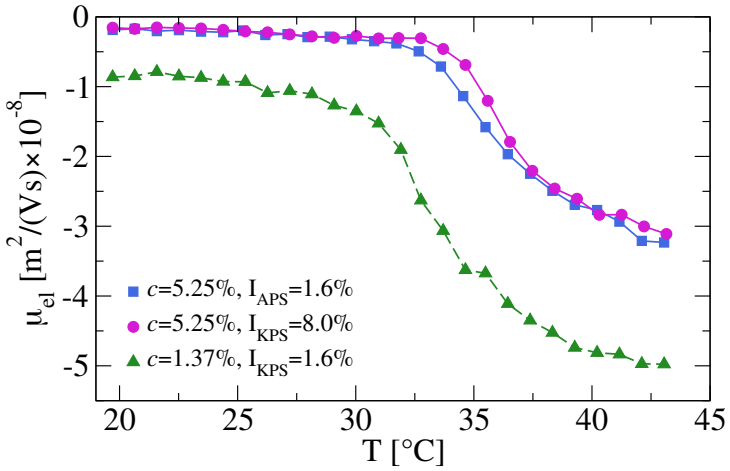

FIG. S1: **Electrophoretic mobility** measurements as a function of temperature T on samples with different size, charge and crosslinker content. The relative error on measurements is less than 5% (not shown).

with increasing initiator concentration while not being affected from the crosslinker concentration. Surprisingly, microgels with different initiator quantities but of roughly the same size show quite similar values of $\mu_{\rm el}$. This may be due to different factors: on one hand, we expect that, for large I_{KPS}, a non-negligible part of the initiator comes out in low molecular weight byproducts, given the high reactivity of these molecules, resulting in a bare charge for final microgels particles which

is lower than the nominal one; on the other hand, the higher the bare charge, the stronger is the electrostatic screening, resulting in an effective charge which is not proportional to the bare one, if not for very low values. Further experiments assessing the dependence of μ_{el} on initiator content in a more systematic fashion would be needed in order to properly understand this behavior, which is beyond the scope of the present work.

Section 3. LOCAL SWELLING IN MONOMERS PROFILES

In Fig. S2 we show the monomer density profiles calculated from simulations of microgels with $c = 1.25\%, 5.0\%$ (top and bottom panels, respectively) and $f = 3.2\%$ randomly distributed charges as a function of α. The coloured regions beneath the curves represent the three different regions used in the analysis of the local swelling of Fig. 3 of the main text, highlighting the core (region I, containing 65% of most inner particles), the inner corona (region II, consisting of 20% of monomers nearest to the core beads) and the outer corona (region III, comprising the 15% most

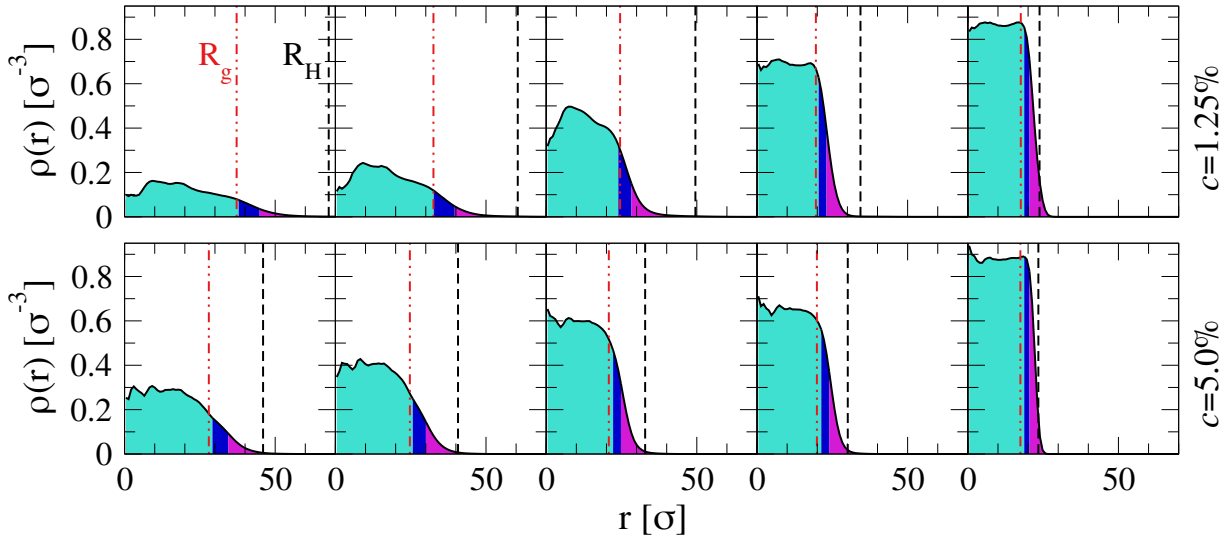

FIG. S2: **Local swelling profiles.** Monomer density profiles for a microgel with $c = 1.25\%$ and $f = 3.2\%$ randomly distributed charges (top panels) for effective temperature values $\alpha = 0, 0.48, 0.74, 0.90, 1.20$, and for a a microgel with $c = 5.0\%$ and $f = 3.2\%$ randomly distributed charges (bottom panels) for effective temperature values $\alpha = 0, 0.48, 0.74, 0.80, 1.20$. The different colors indicate the monomers corresponding to the three regions considered for the analysis of the local swelling, region I (cyan), region II (blue) and region III (magenta). Vertical lines indicate R_g (red, dash-dotted) and R_H (black dashed) values.

exterior beads) of the microgels. Representative snapshots corresponding to microgels in each panel of the figure are shown in Fig. 4 of the main text. As it can be seen, the gyration radius R_g roughly corresponds to the extension of the core region at all c and α values, sharing similar swelling properties as evident from Fig. 3 of the main text, while the hydrodynamic radius R_H embeds also the corona regions, and its value is clearly dependent on the extension of the outer chains, with differences among the cases $c = 1.25\%$ and $c = 5.0\%$.

For completeness, we note that the non-monotonicities observable at low-distance are due to the fact that these data are not averaged over multiple initial configurations. They would be removed by considering several microgel topologies, as shown in our previous works[5], and do not affect the local swelling discussion.

Section 4. CHAIN LENGTH DISTRIBUTIONS

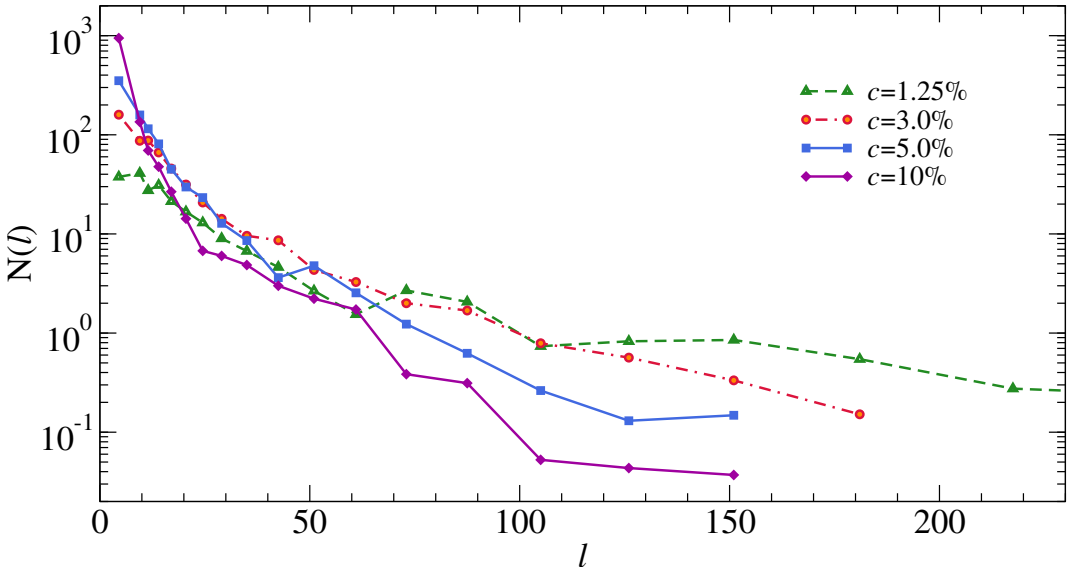

FIG. S3: **Chain length distributions** for microgels with different crosslinker concentrations c.

Fig. S3 shows the number distribution of the chain length l of the microgels. The behavior of all the curves is consistent with a superposition of two exponential distributions, one for low l values, mainly accounting for the chains in the core region, and another for high values of l, which is mostly given by the long chains that can be found in the corona of the microgels. This is due to the radial distribution of the crosslinkers used in the assembly process of the network topology[5], with the aim to realistically mimic the mass distribution of microgels. Of course, it is evident

that as c decreases, small chains become less and less populated while longer chains increase in number and also in length. Again, the noise of the data at large l would be easily improved by considering averages over miltuple microgel topologies, as already done in Ref.[5].

Section 5. LOCAL SWELLING FOR SURFACE CHARGED MICROGELS

For completeness, we report in Fig. S4 the snapshots showing the local swelling of surface-charged microgels for $c = 1.25\%$ and $c = 5\%$ with a charge fraction $f = 0.032$.

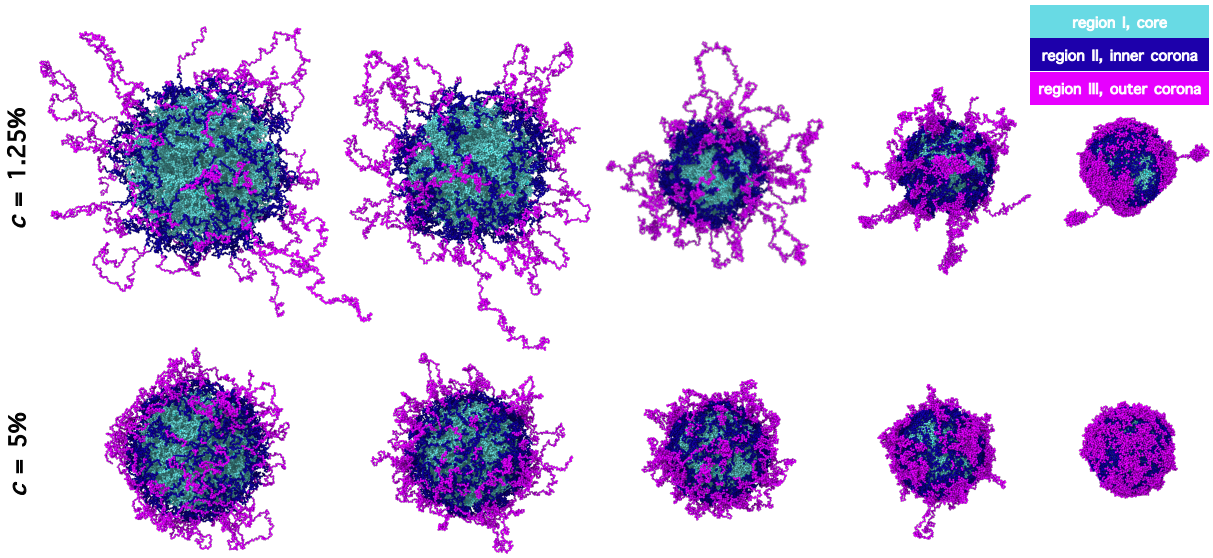

FIG. S4: **Snapshots of surface charged microgels across the VPT illustrating the local swelling.** Simulation snapshots for a surface-charged microgel ($f = 3.2\%$) for different values of the swelling parameter α from the swollen to the collapsed state. From left to right, for $c = 1.25\%$, $\alpha = 0.0, 0.48, 0.80, 0.90, 1.20$, while for $c = 5\%$, $\alpha = 0.0, 0.48, 0.74, 0.90, 1.20$. Monomers are colored according to the region they belong to: cyan indicate the core region (defined as 65% of most inner particles), blue the inner corona region (consisting of 20% of monomers nearest to the core beads) and purple the outer corona region (comprising the 15% most exterior beads).

Section 6. EFFECT OF CHARGES FRACTION

In Fig. S5 we show the swelling curves of R_g and R_H for randomly charged microgels, whose ratio R_g/R_H is reported in Fig. 5(a) of the main text. The swollen size of microgels and the transition temperature α_c increase as f increases, as shown in previous studies. The swelling ratio, defined as the ratio between the swollen and the collapsed radius, is found to be inversely proportional to c, as expected.

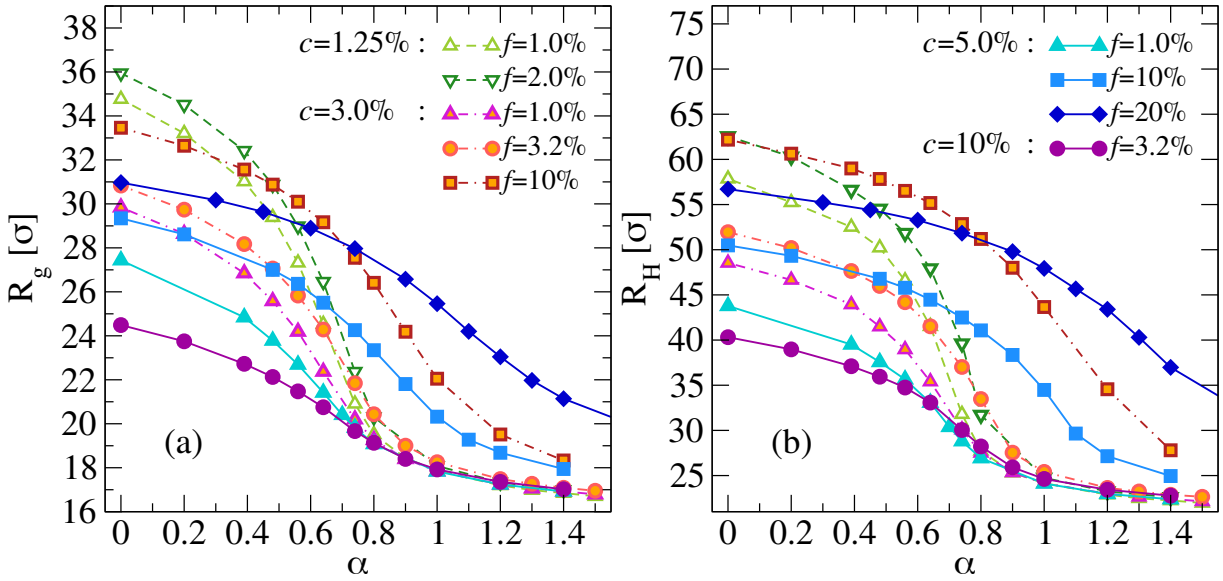

FIG. S5: **Swelling curves for randomly charged microgels**. R_g and R_H swelling curves for randomly charged microgels with different crosslinker (c) and charge (f) content.

Section 7. CHARGED MONOMERS DISTRIBUTIONS IN MICROGELS WITH CHARGES ON THE SURFACE

In Fig. S6 we show the radial distribution of charged monomers in the four kinds of surface charges distributions with $f = 3.2\%$ displayed in Fig. 6 of the main text.

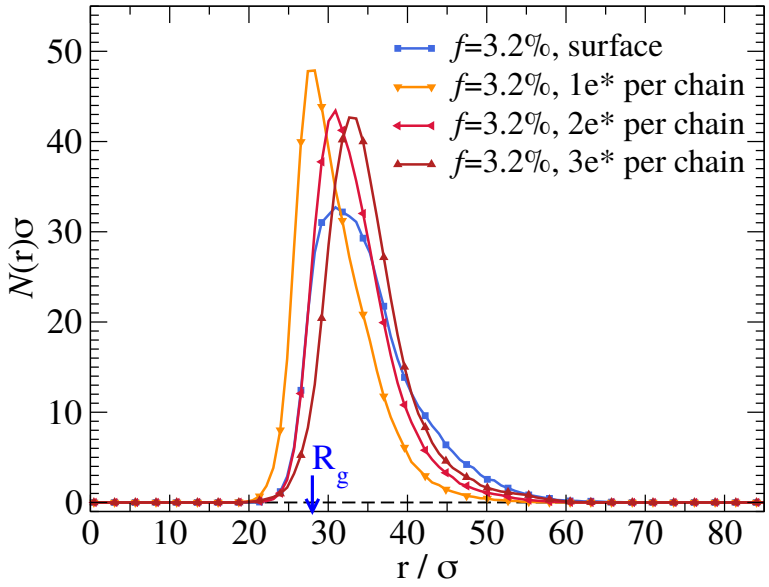

FIG. S6: **Charged monomers radial distributions** of surface charged microgels with crosslinker concentration $c = 5.0\%$ and charges fraction $f = 3.2\%$. Different ways of distributing charged beads on the microgels' surface are considered.

Section 8. EFFECT OF CHARGE DISTRIBUTION

Fig. S7 shows the swelling curves of R_g and R_H for surface charged microgels whose ratio R_g/R_H is displayed in Fig. 6 of the main text. Different ways to distribute charged beads on the microgels' corona are considered. We report the case of standard surface-charged microgels, for which charges are randomly distributed in the region $r > R_g$ on a neutral equilibrated configuration with the constraint that two consecutive beads on a chain cannot both be charged. In addition, we consider $f = 3.2\%$ microgels in which charges are distributed in a constant number for each chain on the most exterior chains. As we can notice, R_g is almost not affected by the charge distribution, while R_H significantly increases as the number of charges per chain grows. We also consider, for the highly charged case ($f = 10\%$) the case in which half of the charges are distributed randomly

throughout the network, half on the surface (mixed distribution, also reported in Fig. 6 of the main text). Also in this case the distribution has a negligible effect on the swelling properties of R_g , while having a strong effect on R_H , for which we cannot observe a transition in the range of examined α values.

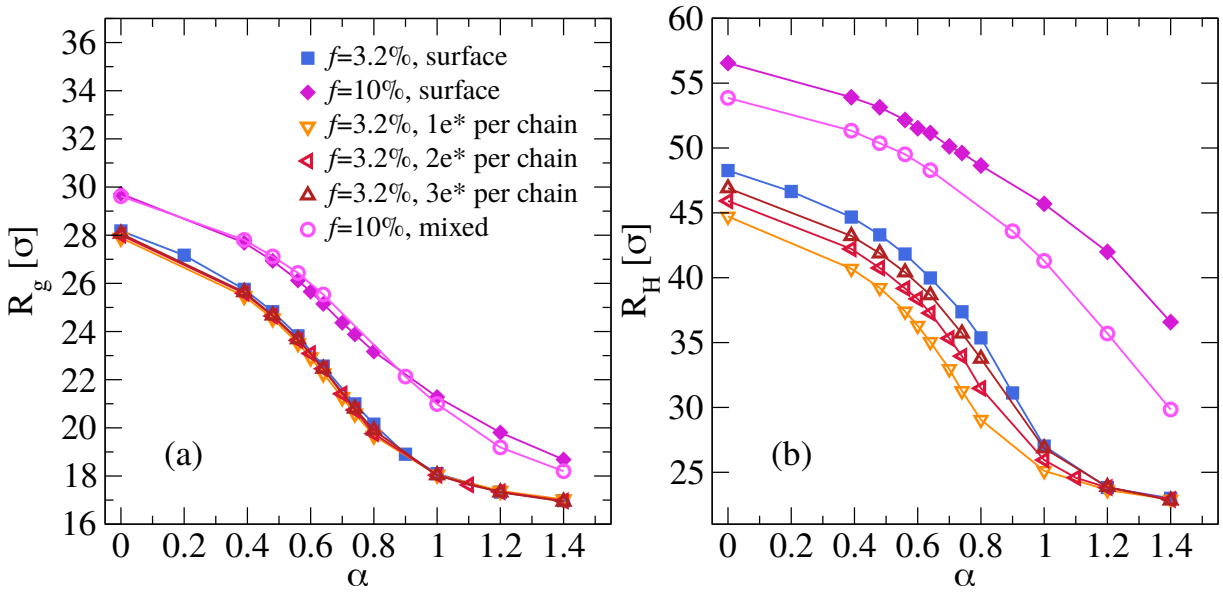

FIG. S7: **Swelling curves of surface charged microgels**. R_g and R_H swelling curves for surface charged microgels with crosslinker concentration $c = 5.0\%$ and charges fractions $f = 3.2\%, 10\%$. Different ways of distributing charged beads on the microgels' surface are considered.

Section 9. GUINIER PLOTS AND CUMULANTS ANALYSIS

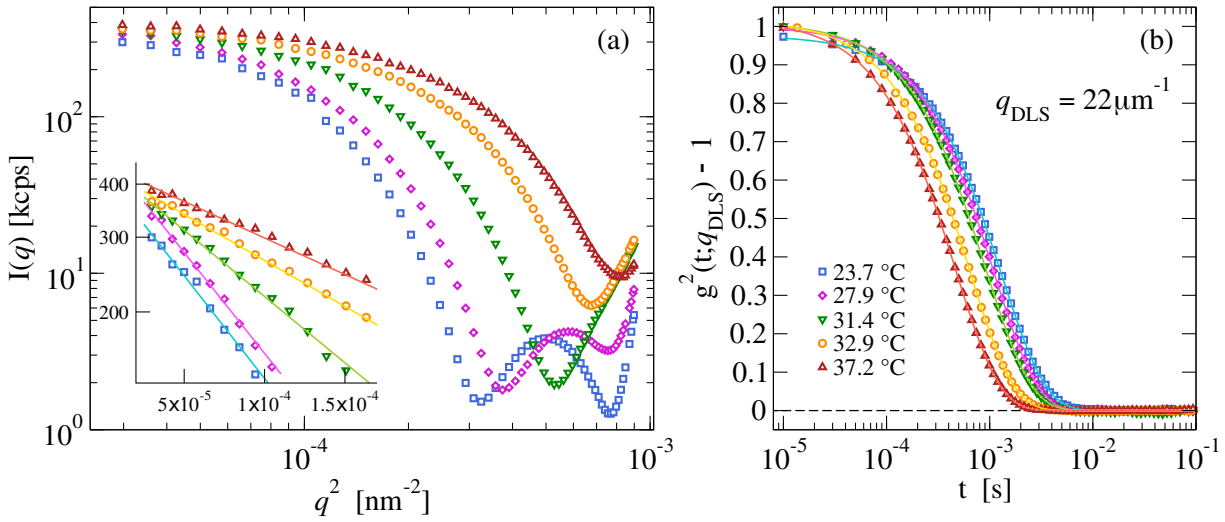

FIG. S8: **SLS and DLS measurements.** (a) Intensity I(q) scattered by a sample of microgels with $c = 5.25$mol% and $I_{\mathrm{APS}} = 1.6$mol% prepared as detailed in the main text at different temperatures across the VPT. Here $q = 4\pi n_0 \sin(\theta/2)/\lambda$ is the magnitude of the scattering vector, θ the scattering angle, $\lambda = 532$nm is the wavelength of the laser beam, and $n_0 = 1.33$ the refractive index of the sample. The inset shows the low-q part of the scattering intensity, where the Guinier regime is attained. The solid lines are non-linear regressions obtained via Eq. 1 of the main text. (b) Intensity autocorrelation functions $g^2(t;q_{\mathrm{DLS}}) - 1$, proportional to the intermediate scattering functions $F_s(q_{\mathrm{DLS}},t)$, measured at $q_{\mathrm{DLS}} = 22\mu\mathrm{m}^{-1}$; solid lines are the best fits obtained via Eq. 3 of the main text. Temperatures for both datasets are indicated in panel (b).

Section 10. ON THE ESTIMATE OF R_H

As reported in the main text, the hydrodynamic radius R_H is a measure of the diffusivity of the particles, that is defined as the radius of a spherical particle moving in a continuous viscous fluid with small Reynolds number (Stokes radius):

$$R_H = \frac{k_B T}{6\pi\eta D} \tag{2}$$

where D is the long-time diffusion coefficient, $k_B T$ the thermal energy, and η the dynamic viscosity. For suspensions of Hard Spheres (HS) R_H roughly corresponds to the geometrical radii of the particles, while for polymeric soft particles, for which a sharp geometrical surface cannot be

defined, it still depends on the extension of the external polymeric chains and their density. Since in our simulations with implicit solvent treatment the diffusion coefficient cannot be computed, and simulations in explicit solvent (with even coarse-grained particles) are out of our disposal of computing resources, we are left to estimate R_H from static equilibrium properties.

Several approximated methods have been proposed to compute estimated values of R_H from equilibrium configurations of polymeric particles, each with different limitations[6]. All of them consider the solvent as a continuous medium flowing through and around the particles. We did not consider methods based on the approximation of the macromolecule as a continuous porous medium[7,8], since this approximation is not suitable for polymeric particles with low chains density in the corona, such as microgels. We also avoided the use of the Kirkwood double-sum formula[9], which does not account for long range correlations in the hydrodynamic force field, and it has been applied successfully only to simple polymer chains. The most accurate methods for estimating the hydrodynamic radius are based on numerical or approximated steady-state solutions of the Navier-Stokes equations for ensembles of spherical bead scatterers[10,11], which are highly computationally demanding for large sized macromolecules. In any case, for systems such as microgels, the main effect on the diffusivity of the particles is given by the polymer chains on the corona, hence it is convenient to define a particle surface[6] and then estimate R_H as the hydrodynamic radius associated to that shape. In this work we pursue that way, which represents a trade-off among accuracy and computational feasibility.

Here we show the comparison among three methods to compute R_H by defining an effective surface for the microgel. For the first one we approximate the microgel as a sphere of radius R_H^ρ such that the equilibrium monomers density profile assumes the value $\rho(R_H^\rho) = 10^{-3}\sigma^{-3}$ at this distance from the center of mass, as also done in a previous work[5]. This definition results to be rough as compared to the other two methods, because it does not account for thermal and shape fluctuations. For the other two methods we compute for each equilibrium configuration a surface mesh, approximating the microgel as a hard ellipsoid having the same gyration tensor of the surface faces, of which we compute the hydrodynamic radius as explained in the main text. The difference among them consists in the way the surface mesh is constructed. In one case the convex hull has been computed, obtaining the estimated hydrodynamic radius R_H^{ch}, which is the value used in the computations of the main text. The other case involves the computation of the surface mesh with the Alpha-shape method[12], which is based on a Delaunay tassellation of the microgels' beads, thereby the space regions are considered as empty or occupied whether the

radius of a circumscribing sphere is greater or smaller than a certain probing radius r_p, after that a surface mesh is constructed. At the same way, from this surface mesh (computed exploiting the Ovito python package) is obtained the hydrodynamic radius estimate R_H^{As}, which obviously depends on the probing sphere radius r_p. The last two methods lead to comparable results, but the convex hull method is parameter-free and the values of the ratio R_g/R_H^{ch} at small and large values of the solvophobic parameter α seems to be more in agreement with the experimental observations, hence we decided to use that method throughout the manuscript.

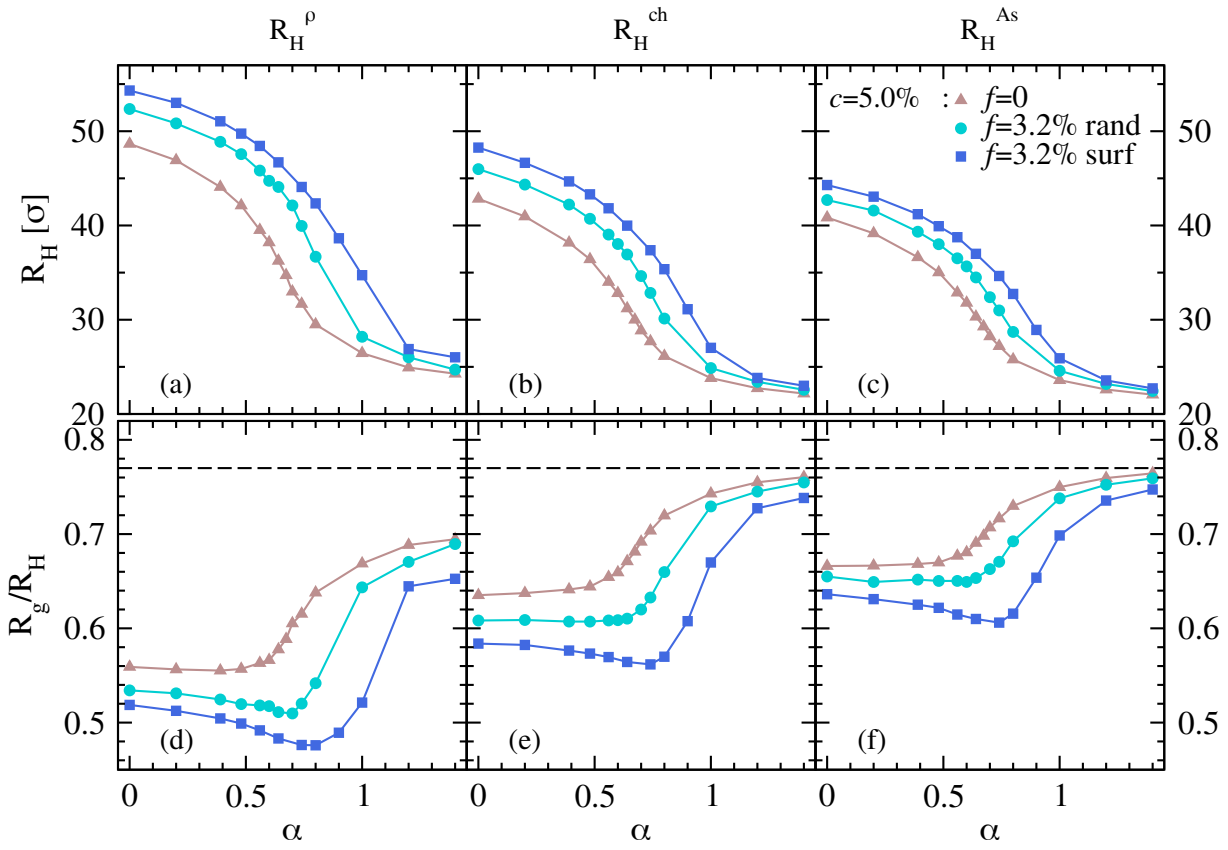

FIG. S9: **Comparison among different estimates of R_H .** Top panels show the hydrodynamic radius as a function of the solvophobic parameter α for microgels with c=5.0%. We consider neutral ones and those with charge content $f = 3.2\%$, distributed both randomly and onto the surface. According to the methods described in the text, the different panels report: R_H^{ρ} (a), R_H^{ch} (b) and R_H^{As} (c). Bottom panels show the corresponding values of R_g/R_H. The surface mesh used to calculate R_H^{As} (c,f) has been constructed using a probing radius of 12σ.

In Fig. S9 we show the comparison among the three methods by observing the different estimates of R_H (top panels) and the ratio R_g/R_H (bottom panels) on microgels with crosslinker

concentration $c = 5.0\%$ (similar trends are observed for microgels with different values of c, not shown), different charged beads fractions ($f = 0, 3.2\%$) and charge distributions (random, surface). The calculation of R_H^ρ is found to be less accurate with respect to the other two methods, due to the low statistics of monomers for densities $\rho(r) \sim 10^{-3}\sigma^{-3}$, well in the outer corona region. In addition, the other two methods both tend to the correct HS value for R_g/R_H at large α. Importantly, all three methods give an overall qualitatively similar behavior, with the onset of a minimum in R_g/R_H for microgel with surface arrangement of charges, while the neutral microgel does not show such a minimum for all three definitions of hydrodynamic radius.

Section 11. CHARGES SCREENING

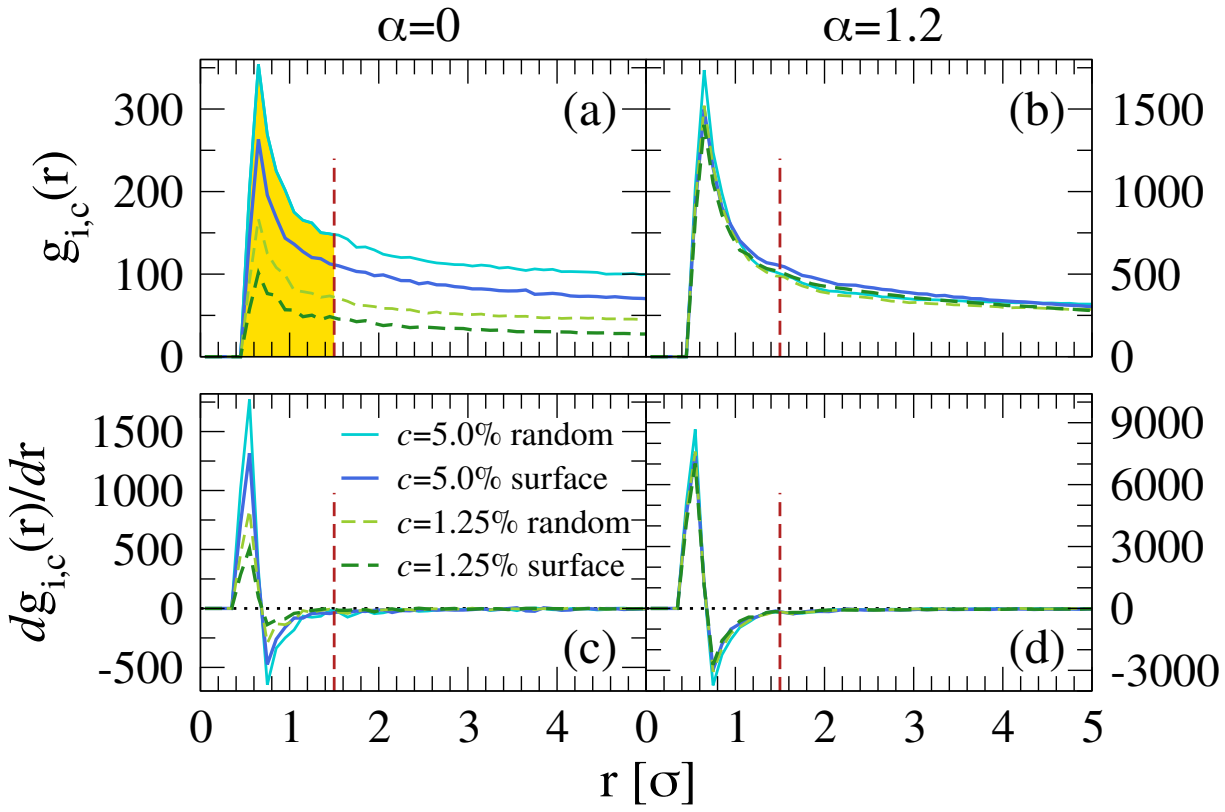

FIG. S10: $g_{i,c}(r)$ **of ions and counterions.** (a,b) cross radial distribution functions $g_{i,c}(r)$ for ions and counterions for random and surface charged microgels with $c = 1.25\%, 5.0\%$ and $f = 3.2\%$ at $\alpha = 0$ and $\alpha = 1.20$. (c,d) Derivative of $g_{i,c}(r)$ with respect to r shown in the top panels.

In the top panels of Fig. S10 the cross radial distribution functions $g_{i,c}(r)$ for ions and counterions are shown, for the swollen (a) and the collapsed (b) state. The vertical dashed line indicates

the cutoff value of $r^* = 1.5$, that we used to calculate the screened charge per chain used to predict the presence of the minimum in R_g/R_H , shown in Fig. 8 of the main text. As we see from the bottom panels in Fig. S10(c,d), r^* roughly indicates the distance at which the derivative of $g_{i,c}(r)$ becomes roughly zero. Integrating $g_{i,c}(r)$ up to r^* we estimate the amount of counterions which can be considered as "bounded" to charged beads, that we use to compute the effective charges $q_{\rm ch}^{\rm eff}$.

REFERENCES

[1]C. G. Lopez and W. Richtering, "Does flory–rehner theory quantitatively describe the swelling of thermoresponsive microgels?" Soft Matter **13**, 8271–8280 (2017).

[2]G. Del Monte, F. Camerin, A. Ninarello, N. Gnan, L. Rovigatti, and E. Zaccarelli, "Charge affinity and solvent effects in numerical simulations of ionic microgels," Journal of Physics: Condensed Matter **33**, 084001 (2020).

[3]D. Capriles-González, B. Sierra-Martín, A. Fernández-Nieves, and A. Fernández-Barbero, "Coupled deswelling of multiresponse microgels," The Journal of Physical Chemistry B **112**, 12195–12200 (2008).

[4]D. Truzzolillo, S. Sennato, S. Sarti, S. Casciardi, C. Bazzoni, and F. Bordi, "Overcharging and reentrant condensation of thermoresponsive ionic microgels," Soft Matter **14**, 4110–4125 (2018).

[5]A. Ninarello, J. J. Crassous, D. Paloli, F. Camerin, N. Gnan, L. Rovigatti, P. Schurtenberger, and E. Zaccarelli, "Modeling microgels with a controlled structure across the volume phase transition," Macromolecules **52**, 7584–7592 (2019), https://doi.org/10.1021/acs.macromol.9b01122.

[6]M. L. Mansfield, J. F. Douglas, S. Irfan, and E.-H. Kang, "Comparison of approximate methods for calculating the friction coefficient and intrinsic viscosity of nanoparticles and macromolecules," Macromolecules **40**, 2575–2589 (2007).

[7]H. Brinkman, "A calculation of the viscous force exerted by a flowing fluid on a dense swarm of particles," Flow, Turbulence and Combustion **1**, 27–34 (1949).

[8]G. Ooms, P. Mijnlieff, and H. Beckers, "Frictional force exerted by a flowing fluid on a permeable particle, with particular reference to polymer coils," The Journal of Chemical Physics **53**, 4123–4130 (1970).

[9]J. G. Kirkwood, "The general theory of irreversible processes in solutions of macromolecules,"

Journal of Polymer Science Part B: Polymer Physics **34**, 597–610 (1996).

[10]J. W. Swan and G. Wang, "Rapid calculation of hydrodynamic and transport properties in concentrated solutions of colloidal particles and macromolecules," Physics of Fluids **28**, 011902 (2016).

[11]A. Ortega, D. Amorós, and J. G. De La Torre, "Prediction of hydrodynamic and other solution properties of rigid proteins from atomic-and residue-level models," Biophysical journal **101**, 892–898 (2011).

[12]A. Stukowski, "Computational analysis methods in atomistic modeling of crystals," Jom **66**, 399–407 (2014).